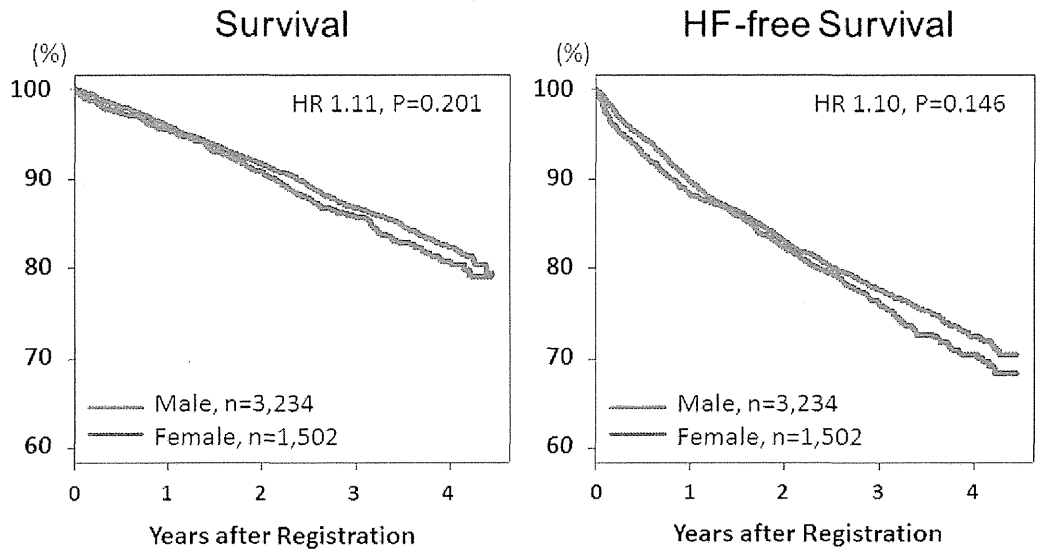

Figure 1. Kaplan-Meier estimates for survival. There were no differences in survival and heart failure (HF)-free survival between female and male patients. HR, hazard ratio.

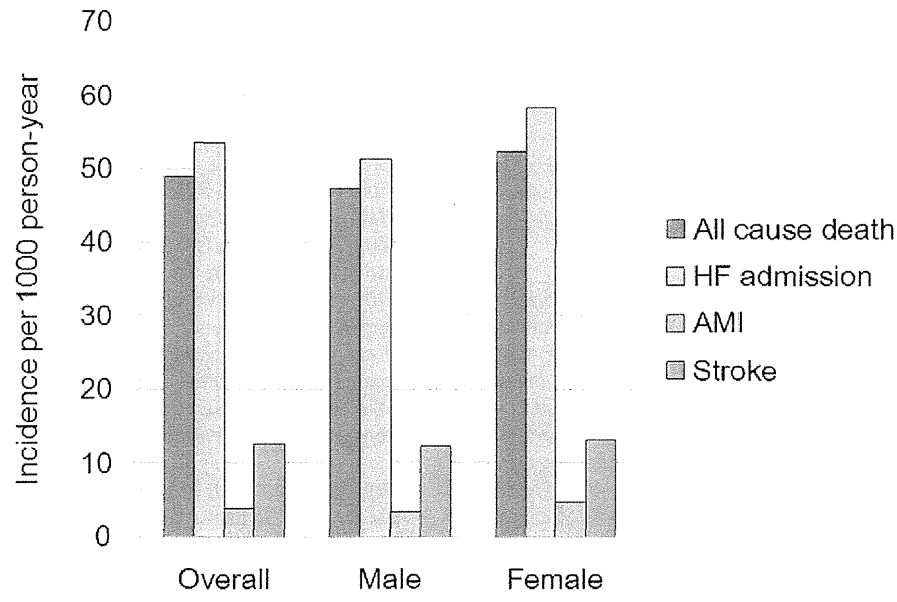

Figure 2. Incidence of all-cause death and cardiovascular event rates. Among the adverse events, death and heart failure (HF) requiring admission were most frequent. Rates of each event were similar between the genders during the median follow-up of 3.1 years (P=0.225, 0.113, 0.293, and 0.678 for all-cause death, HF admission, acute myocardial infarction [AMI], and stroke, respectively).

ysis showed that the prognostic impact of clinical variables on all-cause mortality was similar between the genders (Figure 4).

Discussion

The major findings of the present study are that substantial gender differences exist among Japanese HF patients, and that female CHF patients have better long-term survival compared with male CHF patients after adjustment for clinical parameters, although crude mortality rate was similar between the genders, possibly reflecting the relatively severer clinical manifestation in women. To the best of our knowledge, this is

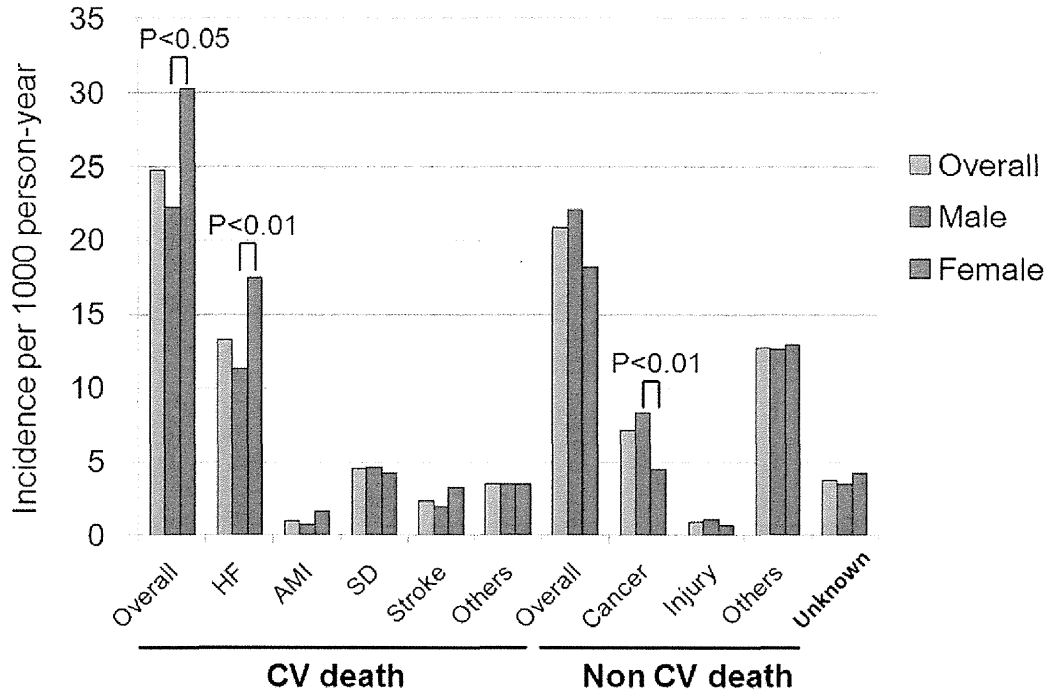

Figure 3. Gender and mode of death. Prevalence of modes of death was different between the genders. Particularly, incidence of death due to heart failure (HF) was more frequent in women, whereas that of malignant disease was more frequent in men. AMI, acute myocardial infarction; CV death, cardiovascular death; non-CV death, non-cardiovascular death; SD, sudden death.

Table 3. Predictors of All-Cause Death, CV Death and HF Admission

	All-cause death			CV death			HF admission		
	HR	95% CI	P-value	HR	95% CI	P-value	HR	95% CI	P-value
Female gender	0.791	0.640–0.979	0.031	1.027	0.767–1.374	0.859	0.858	0.701–1.051	0.139
Age per 10 years	1.568	1.413–1.741	<0.001	1.541	1.333–1.782	<0.001	1.084	0.995–1.181	0.066
BMI	0.955	0.929–0.981	0.001	0.985	0.949–1.022	0.410	1.015	0.991–1.038	0.219
Hypertension	0.894	0.719–1.113	0.316	0.877	0.648–1.188	0.396	1.061	0.857–1.314	0.585
Diabetes mellitus	1.127	0.936–1.358	0.208	0.986	0.756–1.286	0.916	1.249	1.047–1.489	0.013
Dyslipidemia	0.961	0.782–1.181	0.708	1.062	0.790–1.428	0.691	0.794	0.649–0.972	0.025
Smoking	1.168	0.963–1.417	0.114	1.124	0.855–1.478	0.403	0.903	0.749–1.090	0.289
LVEF per 10%	0.988	0.929–1.051	0.704	0.920	0.844–1.003	0.057	0.855	0.806–0.907	<0.001
SBP per 10mmHg	0.954	0.909–1.000	0.052	0.925	0.864–0.989	0.023	0.981	0.937–1.027	0.420
Heart rate per 10beats/min	1.096	1.038–1.157	0.001	1.074	0.994–1.160	0.072	1.040	0.987–1.096	0.146
Hemoglobin	0.882	0.838–0.928	<0.001	0.910	0.848–0.977	0.009	0.866	0.826–0.908	<0.001
Creatinine	1.154	1.082–1.231	<0.001	1.166	1.065–1.277	0.001	0.987	0.906–1.075	0.762
BNP per 100pg/ml	1.494	1.362–1.639	<0.001	1.696	1.484–1.938	<0.001	1.659	1.518–1.813	<0.001
β-blocker	0.826	0.683–0.998	0.048	0.767	0.588–1.000	0.050	0.870	0.726–1.043	0.131
RAS inhibitor	1.054	0.833–1.335	0.661	1.161	0.813–1.660	0.412	1.138	0.887–1.460	0.310
CCB	0.979	0.808–1.186	0.831	1.122	0.857–1.469	0.404	1.019	0.844–1.231	0.843
Statin	0.850	0.682–1.060	0.149	0.975	0.724–1.314	0.869	0.909	0.739–1.118	0.366
Diuretics	1.388	1.133–1.700	0.002	1.874	1.374–2.556	<0.001	2.337	1.878–2.909	<0.001

BMI, body mass index; CCB, calcium channel blocker; CV, cardiovascular; HF, heart failure. Other abbreviations as in Tables 1,2.

the first study to identify gender differences in clinical characteristics, management and long-term outcome in a large CHF cohort in Japan.

Gender Difference in Clinical Characteristics in Japanese CHF Patients

The present study identified gender differences in clinical characteristics, management and long-term outcome in patients

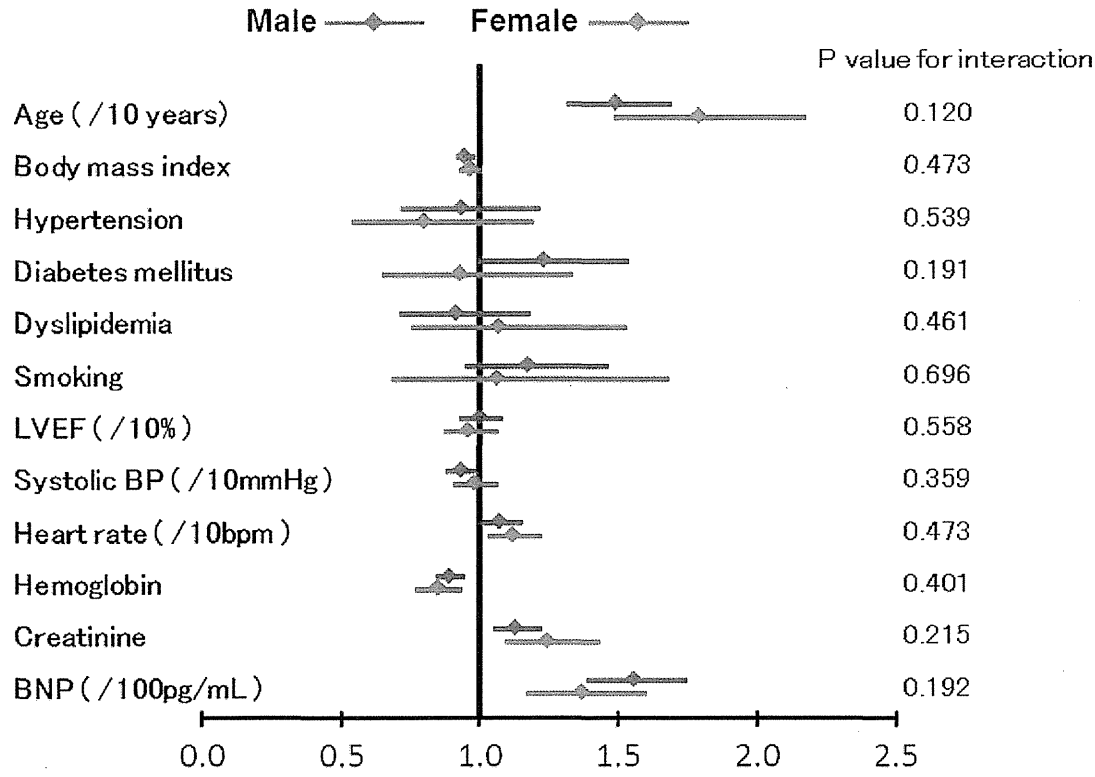

Figure 4. Predictors for all-cause mortality in both genders. Predictors for all-cause mortality were compared between the genders on multivariate Cox proportional hazard modeling. P-value for interaction was significant (P<0.1) for diabetes mellitus. BNP, brain natriuretic peptide; BP, blood pressure; LVEF, left ventricular ejection fractio

with stage C/D HF registered in the CHART-2 study, the largest prospective observational study for HF in Japan. The present results are of great importance given that no studies have comprehensively reported gender differences in HF patients in a large cohort in Japan. We initially found that clinical characteristics were different between the genders in stage C/D HF patients. Particularly, female patients were characterized by higher age, higher prevalence of preserved LVEF, lower prevalence of ischemic heart disease and higher prevalence of valvular heart disease in the present study (Table 1), consistent with previous reports.[9-11] The clinical manifestations of HF appeared to be more severe in women compared with men, in that female patients had a higher NYHA functional class and elevated serum BNP despite the higher prevalence of preserved LVEF (Table 1). Treatment with evidence-based medication (EBM), however, was equally (RASI) or even less frequently (β-blockers and statins) given to women compared with men (Table 2). Thus, it is highly possible that female patients with stage C/D HF are less adequately treated and consequently manifest severer HF conditions compared with male patients. But it is also possible that EBM itself has not been fully established for female patients, who have a higher prevalence of preserved LVEF.[18-26]

Gender Difference in Long-Term Prognosis in Japanese HF Patients

One of the strengths of the present study is that we calculated the incidence of all-cause death and other events by the person-year method. The analysis found that female and male patients with stage C/D HF experienced 52.4 and 47.3 deaths per 1,000 person-years (P=0.225) and 58.3 and 51.3 cases of HF requiring admission per 1,000 person-years (P=0.189), respectively. Thus, there are no gender differences in all-cause death and HF requiring admission, although the incidences of both events are much higher than those of AMI or stroke (Figure 2). Regarding the modes of death in HF patients, the incidence of cardiovascular death, particularly that due to HF, was significantly higher in female patients, whereas that of cancer death was more frequent in male patients (Figure 3). It is thus conceivable that more severe clinical manifestations in female patients resulted in the increased cardiovascular mortality in the present study.

It has been generally accepted that female gender is associated with better survival (either crude and/or age-adjusted) compared with male gender in the broad spectrum of HF.[1-11] Several studies suggested that the gender difference in long-term prognosis of HF could be explained by the higher prevalence of preserved LVEF in women.[4-6] This, however, should be viewed with caution,[9] because gender differences in LVEF in HF patients are due to underlying disease, age and other factors. In the present study, the female CHF patients had better long-term survival than men after adjustment for clinical parameters including LVEF. Thus, unmeasured confounding factors other than LVEF could have affected the better mortality in female CHF patients in the present study.

It is noteworthy that the crude mortality rate did not differ

between the genders in the present study, whereas most of the previous studies reported better crude or unadjusted survival for female CHF patients.[1–3,7–10] One possible explanation for this discrepancy is the higher prevalence of HFpEF in the present study (65.8% for men and 75.1% for women, Table 1), given that similar crude mortality between the genders was also reported in patients with HFpEF enrolled in the ancillary arm of the Digitalis Investigation Group trial.[11] Another explanation would be that female CHF patients might have visited the hospital with a more advanced stage of HF than male CHF patients in the present study, a possible problem in daily practice in Japan.

Life Expectancy in Female CHF Patients

In Japan, the average life expectancy has been increasing in both genders. In 2010, the expectancy at birth was 79.55 years for men and 86.30 years for women,[28] with a 6.35-year difference between the genders that is greater than the 3.8-year difference between the genders in the present study (67.7 vs. 71.5 years, P<0.001). Given that the average life expectancy for a 67.7-year-old Japanese man and 71.5-year-old Japanese women is between 16.44 and 17.20 years, and between 17.73 and 18.58 years in 2010, respectively,[27] women could live an average of approximately 1.5 years longer than men in the general population if their age distribution is similar to that in the present study. The present study, however, found that female CHF patients did not have better survival than men in real-world practice. These lines of evidence suggest that life expectancy was shortened in female HF patients compared with male HF patients in the present study. Further studies are warranted to achieve better HF management based on gender differences, especially for women.

Study Limitations

Several limitations should be mentioned. First, the number of death events was relatively small, which might have limited the power to find significant observations. Second, because all subjects were recruited in the Tohoku district in Japan, caution may be needed when generalizing the present results to other cohorts.

Conclusions

Substantial gender differences were found in clinical characteristics, management and long-term outcome in the present CHART-2 Study. Although women had better survival than men after adjustment for baseline differences, crude mortality rate was similar between the genders, possibly reflecting the relatively severer clinical manifestations in female patients with HF in real-world practice.

Acknowledgments

We thank all the members of the Tohoku Heart Failure Society and the staff of the Departments of Cardiovascular Medicine and Evidence-based Cardiovascular Medicine, Tohoku University Graduate School of Medicine, for their contributions (Appendix). This study was supported by the Grants-in-Aid from the Ministry of Health, Labor, and Welfare (H.S.). H.S. received lecture fees from Bayer Yakuhin (Osaka, Japan), Daiichi Sankyo (Tokyo, Japan) and Novartis Pharma (Tokyo, Japan). The Department of Evidence-based Cardiovascular Medicine, Tohoku University Graduate School of Medicine, is supported in part by the unrestricted research grants from Daiichi Sankyo (Tokyo, Japan), Bayer Yakuhin (Osaka, Japan), Kyowa Hakko Kirin (Tokyo, Japan), Kowa Pharmaceutical (Tokyo, Japan), Novartis Pharma (Tokyo, Japan), Dainippon Sumitomo Pharma (Osaka, Japan), and Nippon Boehringer Ingelheim (Tokyo, Japan).

References

1. McKee PA, Castelli WP, McNamara PM, Kannel WB. Natural history of congestive heart failure: The Framingham Study. *N Engl J Med* 1971; **285:** 1441–1446.
2. Ho KK, Anderson KM, Kannel WB, Grossman W, Levy D. Survival after the onset of congestive heart failure in Framingham Heart Study subjects. *Circulation* 1993; **88:** 107–115.
3. Adams KF, Dunlap SH, Sueta CA, Clarke SW, Patterson JH, Blauwet MB, et al. Relation between gender, etiology and survival in patients with symptomatic heart failure. *J Am Coll Cardiol* 1996; **28:** 1781–1788.
4. Levy D, Kenchaiah S, Larson MG, Benjamin EJ, Kupka MJ, Ho KK, et al. Long-term trends in the incidence of and survival with heart failure. *N Engl J Med* 2002; **347:** 1397–1402.
5. Roger VL, Weston SA, Redfield MM, Hellermann-Homan JP, Killian J, Yawn BP, et al. Trends in heart failure incidence and survival in a community-based population. *JAMA* 2004; **292:** 344–350.
6. Pina IL. A better survival for women with heart failure? It's not so simple. *J Am Coll Cardiol* 2003; **42:** 2135–2138.
7. Adams KF, Sueta CA, Gheorghiade M, O'Connor CM, Schwartz TA, Koch GG, et al. Gender differences in survival in advanced heart failure: Insights from the FIRST study. *Circulation* 1999; **99:** 1816–1821.
8. Ghali JK, Krause-Steinrauf HJ, Adams KF, Khan SS, Rosenberg YD, Yancy CW, et al. Gender differences in advanced heart failure: Insights from the BEST study. *J Am Coll Cardiol* 2003; **42:** 2128–2134.
9. O'Meara E, Clayton T, McEntegart MB, McMurray JJ, Piña IL, Granger CB, et al.; CHARM Investigators. Sex differences in clinical characteristics and prognosis in a broad spectrum of patients with heart failure: Results of the Candesartan in Heart failure: Assessment of Reduction in Mortality and morbidity (CHARM) program. *Circulation* 2007; **115:** 3111–3120.
10. Lam CS, Carson PE, Anand IS, Rector TS, Kuskowski M, Komajda M, et al. Sex differences in clinical characteristics and outcomes in elderly patients with heart failure and preserved ejection fraction: The Irbesartan in Heart Failure with Preserved Ejection Fraction (I-PRESERVE) trial. *Circ Heart Fail.* 2012; **5:** 571–578.
11. Deswal A, Bozkurt B. Comparison of morbidity in women versus men with heart failure and preserved ejection fraction. *Am J Cardiol* 2006; **97:** 1228–1231.
12. Sakata Y, Shimokawa H. Epidemiology of heart failure in Asia. *Circ J* 2013; **77:** 2209–2217.
13. Shiba N, Nochioka K, Miura M, Kohno H, Shimokawa H; CHART-2 Investigators. Trend of westernization of etiology and clinical characteristics of heart failure patients in Japan: First report from the CHART-2 study. *Circ J* 2011; **75:** 823–833.
14. Miura M, Shiba N, Nochioka K, Takada T, Takahashi J, Kohno H, et al; CHART-2 Investigators. Urinary albumin excretion in heart failure with preserved ejection fraction: An interim analysis of the CHART 2 study. *Eur J Heart Fail* 2012; **14:** 367–376.
15. Nochioka K, Sakata Y, Takahashi J, Miyata S, Miura M, Takada T, et al; CHART-2 Investigators. Prognostic impact of nutritional status in asymptomatic patients with cardiac diseases: A report from the CHART-2 Study. *Circ J* 2013; **77:** 2318–2326.
16. Miura M, Sakata Y, Miyata S, Nochioka K, Takada T, Tadaki S, et al.; CHART-2 Investigators. Usefulness of combined risk stratification with heart rate and systolic blood pressure in the management of chronic heart failure: A report from the CHART-2 Study. *Circ J* 2013; **77:** 2954–2962.
17. Yancy CW, Jessup M, Bozkurt B, Butler J, Casey DE Jr, Drazner MH, et al. 2013 ACCF/AHA Guideline for the Management of Heart Failure: A Report of the American College of Cardiology Foundation/American Heart Association Task Force on Practice Guidelines. *J Am Coll Cardiol* 2013; **62:** e147–e239.
18. Yusuf S, Pfeffer MA, Swedberg K, Granger CB, Held P, McMurray JJV, et al. Effects of candesartan in patients with chronic heart failure and preserved left-ventricular ejection fraction: The CHARM Preserved Trial. *Lancet* 2003; **362:** 777–781.
19. Cleland JGF, Tendera M, Adamus J, Freemantle N, Polonski L, Taylor J. The Perindopril in Elderly People with Chronic Heart Failure (PEP-CHF) study. *Eur Heart J* 2006; **27:** 2338–2345.
20. Massie BM, Carson PE, McMurray JJ, Komajda M, McKelvie R, Zile MR, et al. Irbesartan in patients with heart failure and preserved ejection fraction. *N Engl J Med* 2008; **359:** 2456–2467.
21. van Veldhuisen DJ, Cohen-Solal A, Bohm M, Anker SD, Babalis D, Roughton M, et al. Beta-blockade with nebivolol in elderly heart failure patients with impaired and preserved left ventricular ejection fraction: Data from SENIORS (Study of Effects of Nebivolol Intervention on Outcomes and Rehospitalization in Seniors With Heart

Failure). *J Am Coll Cardiol* 2009; **53:** 2150–2158.
22. Hernandez AF, Hammill BG, O'Connor CM, Schulman KA, Curtis LH, Fonarow GC. Clinical effectiveness of beta-blockers in heart failure: Findings from the OPTIMIZE-HF (Organized Program to Initiate Lifesaving Treatment in Hospitalized Patients with Heart Failure) Registry. *J Am Coll Cardiol* 2009; **53:** 184–192.
23. Farasat SM, Bolger DT, Shetty V, Menachery EP, Gerstenblith G, Kasper EK, et al. Effect of beta-blocker therapy on rehospitalization rates in women versus men with heart failure and preserved ejection fraction. *Am J Cardiol* 2010; **105:** 229–234.
24. Yamamoto K, Origasa H, Hori M; J-DHF Investigators. Effects of carvedilol on heart failure with preserved ejection fraction: The Japanese Diastolic Heart Failure Study (J-DHF). *Eur J Heart Fail* 2013; **15:** 110–118.
25. Takano H, Mizuma H, Kuwabara Y, Sato Y, Shindo S, Kotooka N, et al; PEARL Study Investigators. Effects of pitavastatin in Japanese patients with chronic heart failure: The Pitavastatin Heart Failure Study (PEARL Study). *Circ J* 2013; **77:** 917–925.
26. Kihara Y. Statin therapy in chronic heart failure: Frog prince or bare frog? *Circ J* 2013; **77:** 895–897.
27. Ministry of Health, Labour and Welfare of Japan. Complete Life Table. http://www.mhlw.go.jp/toukei/saikin/hw/life/21th/index.html (accessed 25 November, 2013).

Appendix

CHART-2 Study Investigators

1. Executive Committee

Hiroaki Shimokawa (Chair), Toshikazu Goto, Eiji Nozaki, Tetsuya Hiramoto, Mitsumasa Fukuchi, Kanichi Inoue, Atsushi Kato, Masafumi Sugi, Masatoshi Ohe, Tsuyoshi Shinozaki, Satoru Horiguchi, Hiroshi Kato.

2. Steering Committee

Kanichi Inoue, Tetsuya Hiramoto, Masahiko Ogata, Atsushi Kato, Shoichi Sato, Masafumi Sugi.

3. Collaborating Hospitals and Active Investigators by Prefecture

Aomori Prefecture

Shigeto Oyama (Towada City Hospital).

Iwate Prefecture

Eiji Nozaki, Akihiro Nakamura, Tohru Takahashi, Hideaki Endo, Sota Nakajima (Iwate Prefectural Central Hospital). Makoto Nakagawa, Tetsuji Nozaki, Takuya Yagi (Iwate Prefectural Isawa Hospital).

Akita Prefecture

Satoru Horiguchi, Etsuko Fushimi, Yoshinao Sugai, Kohei Fukahori, Satoru Takeda, Kentaro Aizawa (Hiraka General Hospital).

Yamagata Prefecture

Masatoshi Ohe, Katsuhiko Sakurai, Takuro Tashima, Tadashi Kobayashi (Kojirakawa Shiseido Hospital). Toshikazu Goto, Tomoyasu Yahagi, Motoyuki Matsui, Yoshiaki Tamada, Akio Fukui, Kentaro Takahashi, Katsuaki Takahashi, Yoku Kikuchi (Yamagata Prefectural Central Hospital).

Miyagi Prefecture

Akihiko Sugimura, Minako Wakayama, Junko Ohashi (Sendai Red Cross Hospital). Kotaro Nochioka (Kanagami Hospital). Hiroyuki Kanno, Junji Kaneko (Katta General Hospital). Shu Suzuki, Kikuyo Takahashi (KKR Tohoku Kosai Hospital). Kenjiro Akai (Kurihara Central Hospital). Dai Katayose (Miyagi Rifu Ekisaikai Hospital). Sachio Onodera, Tetsuya Hiramoto, Seiji Komatsu, Masanobu Chida, Kaoru Iwabuchi, Masaharu Takeuchi, Hirokazu Yahagi (Osaki Citizen Hospital). Keiji Otsuka, Yoshito Koseki, Masaki Morita (Saito Hospital). Tsuyoshi Shinozaki, Takeshi Ishiduka, Noriko Onoue, Nobuhiro Yamaguchi (Sendai Medical Center). Atsushi Kato, Shigeto Namiuchi, Tadashi Sugie, Kenya Saji, Toru Takii (Sendai Open Hospital). Mitsumasa Fukuchi, Masahiko Ogata, Toshinori Tanikawa, Osamu Kitamukai (Sendai Tokushukai Hospital). Yoshihiro Fukumoto (Shizugawa Public Hospital). Kanichi Inoue, Jiro Koyama, Tomoko Tomioka, Yuki Shioiri, Yoshitaka Ito (South Miyagi Medical Center). Hiroshi Kato, Chikako Takahashi (Tohoku Rosai Hospital). Yasuhiko Sakata, Yoshihiro Fukumoto, Kenta Ito, Masaharu Nakayama, Koji Fukuda, Jun Takahashi, Yuji Wakayama, Koichiro Sugimura, Kimio Sato, Yasuharu Matsumoto (Tohoku University Hospital).

Fukushima Prefecture

Masafumi Sugi, Yoshito Yamamoto, Sunao Toda, Yutaka Minatoya, Yusuke Takagi (Iwaki Kyoritsu Hospital). Koji Fukuda (Watanabe Hospital).

4. Head Office and Coordinating Center

Yasuhiko Sakata, Jun Takahashi, Satoshi Miyata, Kotaro Nochioka, Masanobu Miura, Tsuyoshi Takada, Soichiro Tadaki, Chiharu Saga, Junko Suenaga, Hiromi Mihara, Yoko Yamada, Junko Kimura, Hiromi Ogino, Izumi Oikawa, Sanae Watanabe, Miki Washio, Keiko Nagasawa, Sachiko Nagasawa, Sachie Kotaka, Wakiko Komatsu, Reiko Hashimoto, Madoka Saga, Yasuko Ikeno, Hiroko Hamada.

LETTER

doi:10.1038/nature10992

Mitochondrial DNA that escapes from autophagy causes inflammation and heart failure

Takafumi Oka[1], Shungo Hikoso[1], Osamu Yamaguchi[1], Manabu Taneike[1,2], Toshihiro Takeda[1], Takahito Tamai[1], Jota Oyabu[1], Tomokazu Murakawa[1], Hiroyuki Nakayama[3], Kazuhiko Nishida[1,2], Shizuo Akira[4,5], Akitsugu Yamamoto[6], Issei Komuro[1] & Kinya Otsu[1,2]

Heart failure is a leading cause of morbidity and mortality in industrialized countries. Although infection with microorganisms is not involved in the development of heart failure in most cases, inflammation has been implicated in the pathogenesis of heart failure[1]. However, the mechanisms responsible for initiating and integrating inflammatory responses within the heart remain poorly defined. Mitochondria are evolutionary endosymbionts derived from bacteria and contain DNA similar to bacterial DNA[2–4]. Mitochondria damaged by external haemodynamic stress are degraded by the autophagy/lysosome system in cardiomyocytes[5]. Here we show that mitochondrial DNA that escapes from autophagy cell-autonomously leads to Toll-like receptor (TLR) 9-mediated inflammatory responses in cardiomyocytes and is capable of inducing myocarditis and dilated cardiomyopathy. Cardiac-specific deletion of lysosomal deoxyribonuclease (DNase) II showed no cardiac phenotypes under baseline conditions, but increased mortality and caused severe myocarditis and dilated cardiomyopathy 10 days after treatment with pressure overload. Early in the pathogenesis, DNase II-deficient hearts showed infiltration of inflammatory cells and increased messenger RNA expression of inflammatory cytokines, with accumulation of mitochondrial DNA deposits in autolysosomes in the myocardium. Administration of inhibitory oligodeoxynucleotides against TLR9, which is known to be activated by bacterial DNA[6], or ablation of *Tlr9* attenuated the development of cardiomyopathy in DNase II-deficient mice. Furthermore, *Tlr9* ablation improved pressure overload-induced cardiac dysfunction and inflammation even in mice with wild-type *Dnase2a* alleles. These data provide new perspectives on the mechanism of genesis of chronic inflammation in failing hearts.

Mitochondrial DNA has similarities to bacterial DNA, which contains inflammatogenic unmethylated CpG motifs[2–4,7,8]. Damaged mitochondria are degraded by autophagy, which involves the sequestration of cytoplasmic contents in a double-membraned vacuole, the autophagosome and the fusion of the autophagosome with the lysosome[9]. Pressure overload induces the impairment of mitochondrial cristae morphology and functions in the heart[10,11]. We have previously reported that autophagy is an adaptive mechanism to protect the heart from haemodynamic stress[5].

DNase II, encoded by *Dnase2a*, is an acid DNase found in the lysosome[12]. DNase II in macrophages has an essential role in the degradation of the DNA of apoptotic cells after macrophages engulf them[13]. In the present study, we hypothesized that DNase II in cardiomyocytes digests mitochondrial DNA in the autophagy system to protect the heart from inflammation in response to haemodynamic stress.

First, we examined the alteration of DNase II activity in the heart in response to pressure overload. In wild-type mice, pressure overload by thoracic transverse aortic constriction (TAC) induced cardiac hypertrophy 1 week after TAC and heart failure 8–10 weeks after TAC[5]. DNase II activity was upregulated in hypertrophied hearts, but not in failing hearts (Supplementary Fig. 1a). Immunohistochemical analysis showed infiltration of $CD45^+$ leukocytes, including $CD68^+$ macrophages in failing hearts (Supplementary Fig. 1b). Then, we stained the heart sections with PicoGreen[14], anti-LAMP2a and anti-LC3 (ref. 15) antibodies, which was used for the detection of DNA, lysosomes and autophagosomes, respectively (Supplementary Figs 1c, d and 2a). We observed PicoGreen- and LAMP2a-positive deposits and PicoGreen- and LC3-positive deposits in failing hearts, but not in hypertrophied hearts, suggesting the accumulation of DNA in autolysosomes in failing hearts.

We crossed mice bearing a $Dnase2a^{flox}$ allele[13] with transgenic mice expressing *Cre* recombinase under the control of the α-myosin heavy chain promoter (α-MyHC)[16], to produce $Dnase2a^{flox/flox}$;α-MyHC-Cre^+ ($Dnase2a^{-/-}$) mice. We used $Dnase2a^{flox/flox}$;α-MyHC-Cre^- littermates ($Dnase2a^{+/+}$) as controls. The resulting $Dnase2a^{-/-}$ mice were born at the expected Mendelian frequency. In $Dnase2a^{-/-}$ mice, we observed a 90.1% reduction in the level of *Dnase2a* messenger RNA (mRNA) and a 95.1% decrease in DNase II activity in purified adult cardiomyocyte preparation (Supplementary Fig. 3a, b). Physiological parameters and basal cardiac function assessed by echocardiography showed no differences between $Dnase2a^{+/+}$ and $Dnase2a^{-/-}$ mice (Supplementary Table 1). These results indicate that DNase II does not appear to be required during normal embryonic development or for normal heart growth in the postnatal period.

To clarify the role of DNase II in cardiac remodelling, $Dnase2a^{-/-}$ mice were subjected to TAC. DNase II activity was upregulated in response to pressure overload in $Dnase2a^{+/+}$ hearts and was lower in sham- and TAC-operated $Dnase2a^{-/-}$ hearts than that in the corresponding controls (Supplementary Fig. 3c). Twenty-eight days after TAC, 57.1% of $Dnase2a^{-/-}$ mice had died, whereas 85.7% of $Dnase2a^{+/+}$ mice were still alive (Fig. 1a). The $Dnase2a^{-/-}$ hearts showed left ventricular dilatation and severe contractile dysfunction 10 days after TAC (Fig. 1b–d and Supplementary Table 2). The lung-to-body weight ratio, an index of lung congestion, was elevated in TAC-operated $Dnase2a^{-/-}$ mice (Fig. 1e). The increases in the heart-to-body weight ratio and cardiomyocyte cross-sectional area by TAC were larger in $Dnase2a^{-/-}$ mice than in $Dnase2a^{+/+}$ mice (Fig. 1e, f). TAC-operated $Dnase2a^{-/-}$ hearts showed massive cell infiltration (Fig. 1f). Immunohistochemical analysis of the hearts showed infiltration of $CD45^+$ leukocytes, including $CD68^+$ macrophages (Supplementary Fig. 4a). The mRNA level of interleukin (IL)-6 (*Il6*) was upregulated, but not other cytokine mRNAs in TAC-operated $Dnase2a^{-/-}$ hearts (Supplementary Fig. 4b). TAC-operated $Dnase2a^{-/-}$ hearts showed intermuscular and perivascular fibrosis with increased

[1]Department of Cardiovascular Medicine, Osaka University Graduate School of Medicine, Suita, Osaka 565-0871, Japan. [2]Cardiovascular Division, King's College London, London SE5 9NU, UK. [3]Department of Clinical Pharmacology and Pharmacogenomics, Graduate School of Pharmaceutical Sciences, Osaka University, Suita, Osaka 565-0871, Japan. [4]Laboratory of Host Defense, WPI Immunology Frontier Research Center, Osaka University, Suita, Osaka 565-0871, Japan. [5]Department of Host Defense, Research Institute for Microbial Diseases, Osaka University, Suita, Osaka 565-0871, Japan. [6]Faculty of Bioscience, Nagahama Institute of Bio-Science and Technology, Nagahama, Shiga 526-0829, Japan.

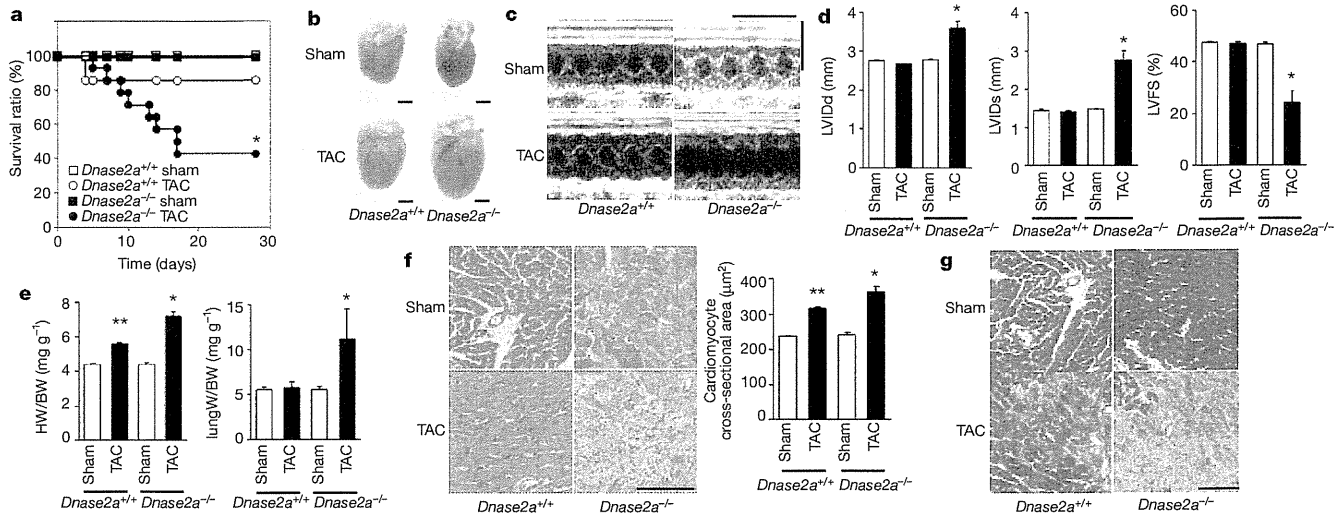

Figure 1 | TAC-induced cardiomyopathy in *Dnase2a*$^{-/-}$ mice. **a**, Survival ratio after TAC ($n = 7$–14 per group). **b**–**g**, Ten days after TAC. **b**, Gross appearance of hearts. Scale bar, 2 mm. **c**, Echocardiography. Scale bars, 0.2 s and 5 mm. Echocardiographic (**d**) and physiological (**e**) parameters ($n = 7$–13 per group). LVIDd and LVIDs, end-diastolic and end-systolic left ventricular internal dimension, respectively; LVFS, left venticular fractional shortening; HW/BW, heart/body weight. Haematoxylin and eosin-stained (**f**) and azocarmine and aniline blue (AZAN)-Mallory-stained (**g**) heart sections. Scale bar, 100 μm. Data are mean ± s.e.m. $^{*}P < 0.05$ versus all other groups, $^{**}P < 0.05$ versus sham-operated controls.

mRNA expression of α2 type I collagen (*Col1a2*) (Fig. 1g and Supplementary Fig. 3d). Ultrastructural analysis of TAC-operated *Dnase2a*$^{-/-}$ hearts showed a disorganized sarcomere structure, misalignment and aggregation of mitochondria, and aberrant electron-dense structures (Supplementary Fig. 4c). The mRNA levels of atrial natriuretic factor (*Nppa*) and brain natriuretic peptide (*Nppb*) were higher in TAC-operated *Dnase2a*$^{-/-}$ mice than in TAC-operated *Dnase2a*$^{+/+}$ mice (Supplementary Fig. 3d). These data suggest that DNase II plays an important role in preventing pressure overload-induced heart failure and myocarditis.

To clarify the molecular mechanisms underlying the cardiac abnormalities observed in *Dnase2a*$^{-/-}$ mice, we evaluated the phenotypes in the earlier time course after pressure overload. Chamber dilation and cardiac dysfunction developed with time after TAC in *Dnase2a*$^{-/-}$ mice (Supplementary Fig. 5a). We chose to perform the analysis 2 days after TAC to minimize the contributions of operation-related events and phenomena secondary to the initial and essential molecular event that induced cardiomyopathy. TAC-operated *Dnase2a*$^{-/-}$ hearts showed cell infiltration without apparent fibrosis (Fig. 2a, b) and infiltration of CD68^{+} macrophages and Ly6G^{+} cells (Fig. 2c). We detected increases in the mRNA levels of IL-1β (*Il1b*) and *Il6*, but not interferon-β (*Ifnb1*) and -γ (*Ifng*) or tumour-necrosis factor (TNF)-α in TAC-operated *Dnase2a*$^{-/-}$ hearts (Supplementary Fig. 6a). To identify the source of IL-1β and IL-6, we performed *in situ* hybridization analysis in heart sections. *Il1b* and *Il6* mRNA-positive cardiomyocytes were evident in TAC-operated *Dnase2a*$^{-/-}$ hearts (Supplementary Fig. 4d).

Ultrastructural analysis showed aberrant electron-dense deposits without apparent changes in sarcomeric and mitochondrial structures

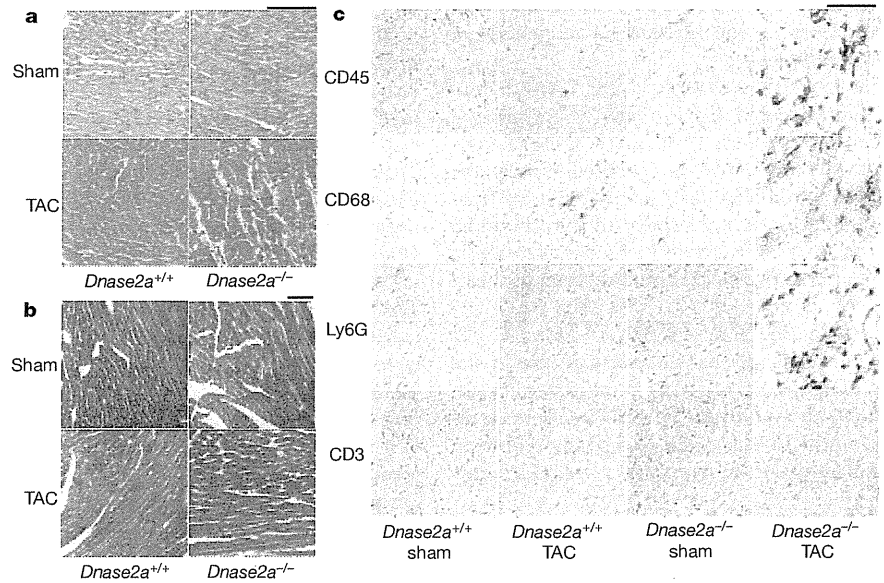

Figure 2 | Pressure overload-induced inflammatory responses in *Dnase2a*$^{-/-}$ mice 2 days after TAC. Mice were analysed 2 days after TAC (**a**–**c**). **a**, Haematoxylin and eosin-stained heart sections. Scale bar, 100 μm. **b**, AZAN-Mallory-stained sections. Scale bar, 100 μm. **c**, Immunohistochemical analysis using antibodies to CD45, CD68, Ly6G and CD3. Scale bar, 100 μm.

in TAC-operated *Dnase2a*$^{-/-}$ hearts (Fig. 3a). At higher magnification, the electron-dense deposits appeared to be autolysosomes (Fig. 3a). Immunoelectron microscopic analysis using anti-DNA antibody showed DNA deposition in autolysosomes (Fig. 3b). In TAC-operated *Dnase2a*$^{-/-}$ hearts, we observed PicoGreen- and LAMP2a-positive deposits and PicoGreen- and LC3-positive deposits (Supplementary Figs 2b and 6b, c). The PicoGreen-positive deposits were not TdT-mediated dUTP nick end labelling (TUNEL)-positive (Supplementary Fig. 6d), indicating that the DNA was not derived from fragmented nuclear DNA. To label mitochondrial DNA, mice were injected with 5-ethynyl-2′-deoxyuridine (EdU) five times before TAC. EdU, a nucleoside analogue to thymidine, is incorporated into DNA during active DNA synthesis[17]. EdU specifically binds to mitochondrial DNA during its active DNA synthesis in non-dividing cardiomyocytes. In TAC-operated *Dnase2a*$^{-/-}$ hearts, we observed EdU- and LAMP2a-positive deposits and EdU- and LC3-positive deposits (Fig. 3c, d and Supplementary Fig. 2c), indicating that mitochondrial DNA accumulated in autolysosomes.

The innate immune system is the major contributor to acute inflammation induced by microbial infection[18]. TLR9, localized in the endolysosome, senses DNA with unmethylated CpG motifs derived from bacteria and viruses. Mitochondrial DNA activates polymorphonuclear neutrophils through CpG/TLR9 interactions[19]. Immunohistochemical analysis indicated that TLR9 was co-localized with EdU-positive deposits (Fig. 3e). TLR9 is activated by synthetic oligodeoxynucleotides (ODN1668) that contains unmethylated CpG[6], but it is inhibited by inhibitory ligands, such as ODN2088 (ref. 20), in which 'GCGTT' in ODN1668 is replaced with 'GCGGG'. ODN1668 induced increases in *Il1b* and *Il6* mRNA levels in wild-type isolated adult cardiomyocytes (data not shown). We, then, examined the effect of ODN2088 on carbonyl cyanide *m*-chlorophenyl hydrazone (CCCP) or isoproterenol-induced cell death using isolated adult cardiomyocytes to eliminate the contribution of immune cells[5]. CCCP, a protonophore, induces dissipation of mitochondrial membrane potential. Isoproterenol caused a loss of mitochondrial membrane potential in wild-type cardiomyocytes, as indicated by loss of tetramethylrhodamine ethyl ester signal (Supplementary Fig. 7a). Incubation with CCCP or isoproterenol induced conversion of LC3-I to LC3-II, an essential step during autophagosome formation, and treatment with the lysosomal inhibitor bafilomycin A1 led to an even larger increase of LC3-II in CCCP- or isoproterenol-treated cells than in control cells, indicating that CCCP or isoproterenol accelerated autophagic flux (Supplementary Fig. 7b). Isolated cardiomyocytes from *Dnase2a*$^{-/-}$ hearts were more susceptible than those from control hearts to CCCP or isoproterenol in the presence of

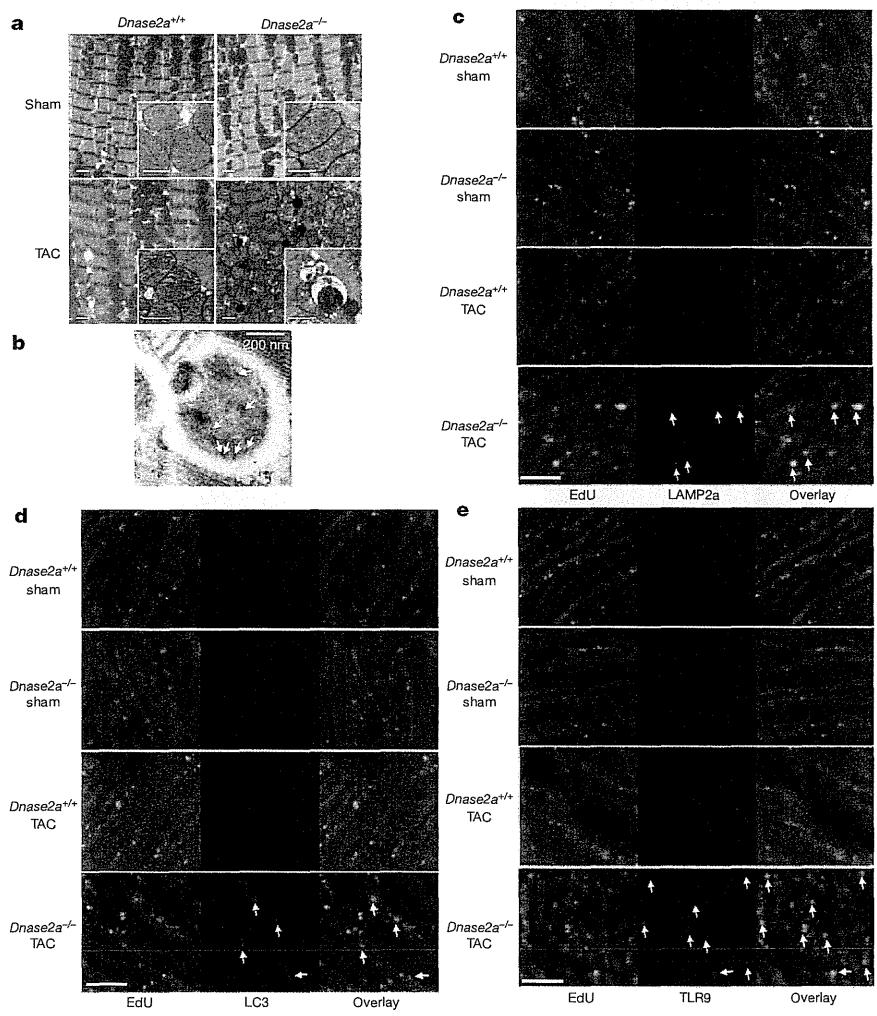

Figure 3 | Deposition of mitochondrial DNA in autolysosomes in pressure-overloaded *Dnase2a*$^{-/-}$ hearts. Mice were analysed 2 days after TAC (**a**–**e**). **a**, Electron microscopic analysis. Images of mitochondria at higher magnification are shown in subsets. Scale bar, 1 μm. **b**, Autolysosome after incubation with anti-DNA antibody and 10 nm gold staining. Scale bar, 200 nm. Arrows indicate labelled DNA. Double staining of heart sections with EdU (green) and anti-LAMP2a antibody (red) (**c**), EdU (green) and anti-LC3 antibody (red) (**d**) or EdU and anti-TLR9 antibody (red) (**e**). Arrows indicate EdU-positive and LAMP2a-, LC3- or TLR9-positive structures. Scale bar, 10 μm.

inactive control oligodeoxynucleotides (ODN2088 control) (Supplementary Fig. 7c–e). CCCP upregulated the mRNA expression levels of *Il1b* and *Il6* in *Dnase2a*$^{-/-}$ cardiomyocytes (Supplementary Fig. 7f). Incubation of *Dnase2a*$^{-/-}$ cardiomyocytes with ODN2088 attenuated the cell death and cytokine mRNA induction by CCCP treatment. Treatment of the *Dnase2a*$^{-/-}$ cardiomyocytes with 3-methyladenine, an autophagy inhibitor, and rapamycin, an autophagy inducer, inhibited and enhanced the induction of the cytokine mRNA by CCCP treatment, respectively (Supplementary Fig. 7g).

We next examined whether the inhibition of TLR9 can rescue the cardiac phenotypes in TAC-operated *Dnase2a*$^{-/-}$ mice. Administration of ODN2088 resulted in the improvement of survival 28 days after TAC (Fig. 4a). ODN2088 attenuated chamber dilation and cardiac dysfunction compared with the control oligodeoxynucleotides 4 days after TAC (Fig. 4b, c and Supplementary Fig. 8a). In addition, ODN2088 inhibited infiltration of CD68^{+} macrophages and Ly6G^{+} cells, fibrosis and upregulation of *Il6*, *Ifng*, *Nppa* and *Col1a2* mRNAs in TAC-operated *Dnase2a*$^{-/-}$ hearts (Fig. 4d and Supplementary Fig. 8b–e). ODN2088 prevented cardiac remodelling for a longer time (end-diastolic left ventricular internal dimension (LVIDd), in millimetres, 2.74 ± 0.03, 2.76 ± 0.03; end-systolic left ventricular internal dimension (LVIDs), in millimetres, 1.37 ± 0.03, 1.34 ± 0.05; left ventricular fractional shortening (LVFS) (%), 50.1 ± 0.7, 51.4 ± 1.5, before and 14 days after TAC, respectively, $n = 6$). Furthermore, ablation of *Tlr9* rescued the cardiac phenotypes in TAC-operated *Dnase2a*$^{-/-}$ mice (Supplementary Fig. 9).

To examine the significance of TLR9 signalling pathway in the genesis of heart failure, we subjected TLR9-deficient mice[6] to TAC. Ten weeks after TAC, TLR9-deficient mice showed smaller left ventricular dimensions, better cardiac function and less pulmonary congestion than in TAC-operated control mice (Fig. 4e, f and Supplementary Fig. 10a). The extent of fibrosis, the levels of *Nppa*, *Nppb* and *Col1a2* mRNA, infiltration of CD68^{+} macrophages were attenuated in TLR9-deficient mice (Supplementary Fig. 10b–e). We detected no significant differences in the cytokine mRNA levels between TAC-operated groups (Supplementary Fig. 10f). Furthermore, ODN2088 improved survival of wild-type mice in a more severe TAC model (Supplementary Fig. 10g). These data indicate that the TLR9 signalling pathway is involved in inflammatory responses in failing hearts in response to pressure overload and plays an important role in the pathogenesis of heart failure.

In this study, we showed that mitochondrial DNA that escapes from autophagy-mediated degradation cell-autonomously leads to TLR9-mediated inflammatory responses in cardiomyocytes, myocarditis and dilated cardiomyopathy. Immune responses are initiated and perpetuated by endogenous molecules released from necrotic cells, in addition to pathogen-associated molecular patterns expressed in invading microorganisms[21]. Cellular disruption by trauma releases mitochondrial molecules, including DNA, into circulation to cause systemic inflammation[19]. Depletion of autophagic proteins promotes cytosolic translocation of mitochondrial DNA and caspase-1-dependent cytokines mediated by the NALP3 inflammasome in response to

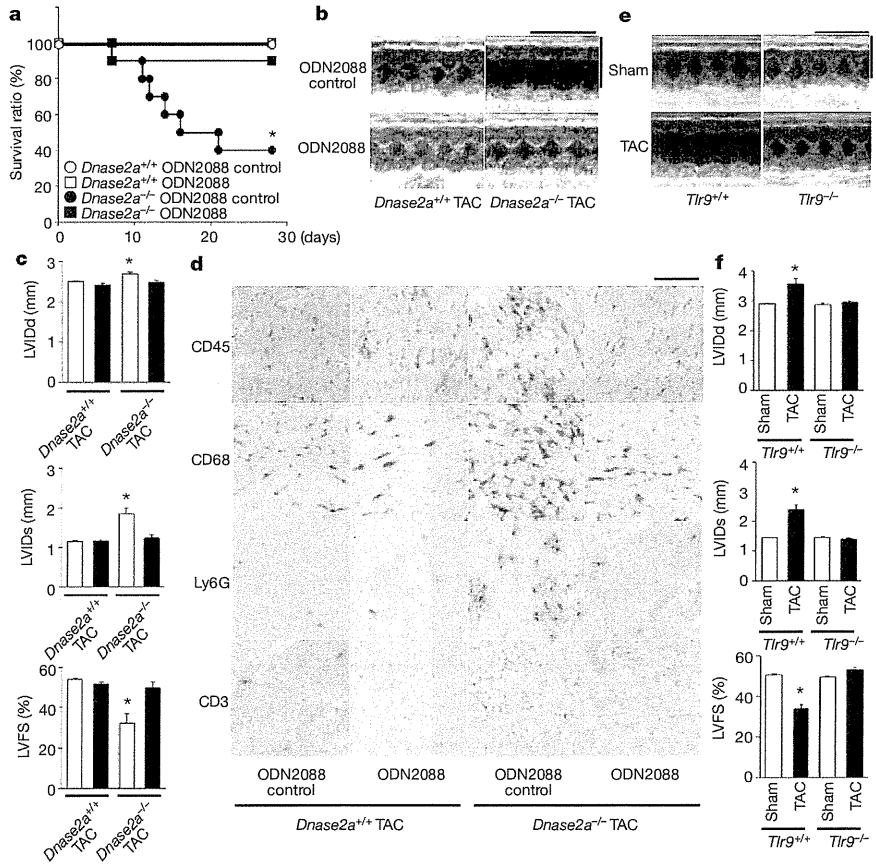

Figure 4 | Inhibition of TLR9 attenuated TAC-induced heart failure. **a**, Survival ratio of TAC-operated ODN-treated mice ($n = 6$–10 per group). **b**–**d**, Four days after TAC. **b**, Echocardiography. Scale bars, 0.2 s and 5 mm. **c**, Echocardiographic parameters. Open and closed bars represent ODN2088 control- and ODN2088-treated groups, respectively ($n = 5$–8 per group). **d**, Immunohistochemical analysis. Scale bar, 100 μm. TLR9-deficient mice were analysed 10 weeks after TAC (**e**, **f**). **e**, Scale bars, 0.2 s and 5 mm. **f**, Echocardiographic parameters ($n = 6$–10 per group). Data are mean ± s.e.m. *$P < 0.05$ versus all other groups.

lipopolysaccharide in macrophages[22]. We observed no significant difference in the amount of mitochondrial DNA in the blood between TAC-operated *Dnase2a*$^{-/-}$ and *Dnase2a*$^{+/+}$ mice (data not shown), excluding a possibility that circulating mitochondrial DNA is causing most of the inflammatory responses mediated by TLR9. The mechanisms presented here do not require release of mitochondrial DNA from cardiomyocytes into extracellular space.

Increased levels of circulating proinflammatory cytokines are associated with disease progression and adverse outcomes in patients with chronic heart failure[1]. Mitochondrial DNA plays an important role in inducing and maintaining inflammation in the heart. This mechanism might work in many chronic non-infectious inflammation-related diseases such as atherosclerosis, metabolic syndrome and diabetes mellitus.

METHODS SUMMARY

Animal study. The study was performed under the supervision of the Animal Research Committee of Osaka University and in accordance with the Japanese Act on Welfare and Management of Animals (No. 105). The 12- to 14-week-old mice were subjected to TAC[5,23] and severe TAC using 26- and 27-gauge needles for aortic constriction, respectively.

Biochemical assays. The DNase II activity was determined by the single radial enzyme-diffusion method[24]. The mRNA levels were determined by quantitative PCR with reverse transcription (RT–PCR)[5].

Histological analysis. The antibodies used were anti-mouse CD45 (ANASPEC), CD68 (Serotec), Ly6G/6C (BD Pharmingen), CD3 (Abcam), DNA (Abcam), LAMP2a (Zymed), LC3 (ref. 25) and TLR9 (Santa-Cruz). The *in situ* hybridization analysis was performed using DIG RNA Labelling Kit and DIG Nucleic Acid Detection Kit (Roche Diagnostics). Hearts were embedded in LR White resin for immunoelectron microscopy[26]. Heart sections were incubated in PicoGreen (Molecular Probes) for 1 h. Twenty-four hours before TAC, mice were injected intraperitoneally with 250 μg of EdU every 2 h five times, and EdU was detected with a Click-iT EdU Alexa Fluor 488 Imaging Kit (Invitrogen).

***In vitro and in vivo* rescue experiments with the TLR9 inhibitor.** Cardiomyocytes[5] were pre-treated with 1 μg ml^{-1} inhibitory CpG (ODN2088) or control (ODN2088 control) oligodeoxynucleotides for 5 h and incubated with 20 nM CCCP or 50 μM isoproterenol for 24 h (ref. 20). The cells were loaded with tetramethylrhodamine ethyl ester (Molecular Probe) at 10 nM for 30 min. The mice were injected intravenously with 500 μg of the oligodeoxynucleotides 2 h before and 2 and 4 days after TAC, and every 3 days thereafter.

Statistical analysis. Results are shown as the mean ± s.e.m. Paired data were evaluated using a Student's *t*-test. A one-way analysis of variance with the Bonferroni post hoc test was used for multiple comparisons. The Kaplan–Meier method with a log-rank test was used for survival analysis.

Full Methods and any associated references are available in the online version of the paper at www.nature.com/nature.

Received 26 June 2011; accepted 1 March 2012.
Published online 25 April 2012.

1. Mann, D. L. Inflammatory mediators and the failing heart: past, present, and the foreseeable future. *Circ. Res.* **91,** 988–998 (2002).
2. Pollack, Y., Kasir, J., Shemer, R., Metzger, S. & Szyf, M. Methylation pattern of mouse mitochondrial DNA. *Nucleic Acids Res.* **12,** 4811–4824 (1984).
3. Cardon, L., Burge, C., Clayton, D. A. & Karlin, S. Pervasive CpG suppression in animal mitochondrial genomes. *Proc. Natl Acad. Sci. USA* **91,** 3799–3803 (1994).
4. Gray, M. W., Burger, G. & Lang, B. F. Mitochondrial evolution. *Science* **283,** 1476–1481 (1999).
5. Nakai, A. *et al.* The role of autophagy in cardiomyocytes in the basal state and in response to hemodynamic stress. *Nature Med.* **13,** 619–624 (2007).
6. Hemmi, H. *et al.* A Toll-like receptor recognizes bacterial DNA. *Nature* **408,** 740–745 (2000).
7. Taanman, J.-W. The mitochondrial genome: structure, transcription, translation and replication. *Biochim Biophys Acta Bioenerget.* **1410,** 103–123 (1999).
8. Collins, L., Hajizadeh, S., Holme, E., Jonsso, I. & Tarkowski, A. Endogenously oxidized mitochondrial DNA induces *in vivo* and *in vitro* inflammatory responses. *J. Leukoc. Biol.* **75,** 995–1000 (2004).
9. Mizushima, N., Levine, B., Cuervo, A. M. & Klionsky, D. J. Autophagy fights disease through cellular self-digestion. *Nature* **451,** 1069–1075 (2008).
10. Meerson, F., Zaletayeva, T., Lagutchev, S. & Pshennikova, M. Structure and mass of mitochondria in the process of compensatory hyperfunction and hypertrophy of the heart. *Exp. Cell Res.* **36,** 568–578 (1964).
11. Bugger, H. *et al.* Proteomic remodelling of mitochondrial oxidative pathways in pressure overload-induced heart failure. *Cardiovasc. Res.* **85,** 376–384 (2010).
12. Evans, C. J. & Aguilera, R. J. DNase II: genes, enzymes and function. *Gene* **322,** 1–15 (2003).
13. Kawane, K. *et al.* Chronic polyarthritis caused by mammalian DNA that escapes from degradation in macrophages. *Nature* **443,** 998–1002 (2006).
14. Ashley, N., Harris, D. & Poulton, J. Detection of mitochondrial DNA depletion in living human cells using PicoGreen staining. *Exp. Cell Res.* **303,** 432–446 (2005).
15. Kabeya, Y. *et al.* LC3, a mammalian homologue of yeast Apg8p, is localized in autophagosome membranes after processing. *EMBO J.* **19,** 5720–5728 (2000).
16. Yamaguchi, O. *et al.* Cardiac-specific disruption of the *c-raf-1* gene induces cardiac dysfunction and apoptosis. *J. Clin. Invest.* **114,** 937–943 (2004).
17. Lentz, S. I. *et al.* Mitochondrial DNA (mtDNA) biogenesis: visualization and duel incorporation of BrdU and EdU into newly synthesized mtDNA *in vitro*. *J. Histochem. Cytochem.* **58,** 207–218 (2010).
18. Takeuchi, O. & Akira, S. Pattern recognition receptors and inflammation. *Cell* **140,** 805–820 (2010).
19. Zhang, Q. *et al.* Circulating mitochondrial DAMPs cause inflammatory responses to injury. *Nature* **464,** 104–107 (2010).
20. Stunz, L. *et al.* Inhibitory oligonucleotides specifically block effects of stimulatory CpG oligonucleotides in B cells. *Eur. J. Immunol.* **32,** 1212–1222 (2002).
21. Bianchi, M. E. DAMPs, PAMPs and alarmins: all we need to know about danger. *J. Leukoc. Biol.* **81,** 1–5 (2007).
22. Nakahira, K. *et al.* Autophagy proteins regulate innate immune responses by inhibiting the release of mitochondrial DNA mediated by the NALP3 inflammasome. *Nature Immunol.* **12,** 222–230 (2011).
23. Yamaguchi, O. *et al.* Targeted deletion of apoptosis signal-regulating kinase 1 attenuates left ventricular remodeling. *Proc. Natl Acad. Sci. USA* **100,** 15883–15888 (2003).
24. Koizumi, T. Deoxyribonuclease II (DNase II) activity in mouse tissues and body fluids. *Exp. Anim.* **44,** 169–171 (1995).
25. Lu, Z. *et al.* Participation of autophagy in the degeneration process of rat hepatocytes after transplantation following prolonged cold preservation. *Arch. Histol. Cytol.* **68,** 71–80 (2005).
26. Mosgoller, W. *et al.* Distribution of DNA in human Sertoli cell nucleoli. *J. Histochem. Cytochem.* **41,** 1487–1493 (1993).

Supplementary Information is linked to the online version of the paper at www.nature.com/nature.

Acknowledgements We thank S. Nagata and K. Kawane, Kyoto University, for discussions and a gift of *Dnase2a*$^{flox/flox}$ mice, and Y. Uchiyama, Juntendo University, for anti-LC3 antibody. We also thank K. Takada for technical assistance. This work was supported by a Grant-in-Aid for Scientific Research from the Ministry of Education, Culture, Sports, Science and Technology in Japan and research grants from Mitsubishi Pharma Research Foundation and the British Heart Foundation (CH/11/3/29051, RG/11/12/29052).

Author Contributions S.A. and I.K. provided intellectual input; K.O. was responsible for the overall study design and writing the manuscript. The other authors performed experiments and analysed data. All authors contributed to the discussions.

Author Information Reprints and permissions information is available at www.nature.com/reprints. The authors declare no competing financial interests. Readers are welcome to comment on the online version of this article at www.nature.com/nature. Correspondence and requests for materials should be addressed to K.O. (kinya.otsu@kcl.ac.uk).

METHODS

Animal study. The study was performed under the supervision of the Animal Research Committee of Osaka University and in accordance with the Japanese Act on Welfare and Management of Animals (No. 105).

We crossed mice bearing a *Dnase2a*^{flox} allele[13] with transgenic mice expressing *Cre* recombinase under the control of the α-myosin heavy chain promoter (α-MyHC)[16], to produce cardiac-specific DNase II-deficient mice, *Dnase2a*$^{flox/flox}$;α-MyHC-*Cre*$^{+}$ (*Dnase2a*$^{-/-}$). To generate double-knockout mice of *Dnase2a* and *Tlr9*, we crossed *Dnase2a*$^{-/-}$ mice with *Tlr9*$^{-/-}$ mice[6].

The 12- to 14-week-old male mice were subjected to TAC[5,23] and severe TAC using 26- and 27-gauge needles for aortic constriction, respectively. Non-invasive measurements of blood pressure were performed on mice anaesthetized with 2.5% avertin using a blood pressure monitor for rats and mice Model MK-2000 (Muromachi Kikai) according to the manufacturer's instructions[5,23]. To perform echocardiography on awakened mice, ultrasonography (SONOS-5500, equipped with a 15 MHz linear transducer, Philips Medical Systems) was used. The heart was imaged in the two-dimensional parasternal short-axis view, and an M-mode echocardiogram of the midventricle was recorded at the level of the papillary muscles. Heart rate, intraventricular septum and posterior wall thickness, and end-diastolic and end-systolic internal dimensions of the left ventricle were obtained from the M-mode image.

Measurement of DNase II activity. The DNase II activity was determined using the single radial enzyme-diffusion method[24]. The heart homogenates were applied to the cylindrical wells (radius, 1.5 mm) punched in 1% (w/v) agarose gel, containing 0.05 mg ml^{-1} salmon sperm DNA (Type III), 5 μg ml^{-1} ethidium bromide, 0.5 M sodium acetate buffer (pH 4.7) and 10 mM EDTA. After incubation for 48 h at 37 °C, the radius of the dark circle was measured under an ultraviolet transilluminator at 312 nm. DNase II activities for the samples were determined using a standard curve constructed from the serial dilution of porcine DNase II (Sigma).

Quantitative RT–PCR. Total RNA was isolated from the left ventricle or cultured cardiomyocytes for analysis using the TRIzol reagent (Invitrogen Life Technologies). The mRNA levels were determined by quantitative RT–PCR[5]. For reverse transcription and amplification, we used the TaqMan Reverse Transcription Reagents (Applied Biosystems) and Platinum Quantitative PCR SuperMix-UDG (Invitrogen Life Technologies), respectively. The PCR primers and probes were obtained from Applied Biosystems. The primers used were as follows: *Nppa* assay identity, mm01255747_g1; *Nppb* assay identity, mm00435304_g1; *Col1a2* assay identity, Mm01165187_m1; *Gapdh* assay identity, 4352339E; *Il6* assay identity, Mm99999064_m1; *Il1b* assay identity, Mm01336189_m1; *Ifnb1* assay identity, Mm00439546_s1; *Ifng* assay identity, Mm99999071_m1; *Tnf* assay identity, Mm00443260_g1; and *Dnase2a* assay identity, Mm00438463_m1. We constructed quantitative PCR standard curves using the corresponding complementary DNA, and all data were normalized to *Gapdh* mRNA content.

Histological analysis. Heart samples were excised and immediately fixed in buffered 4% paraformaldehyde, embedded in paraffin and cut into 5 μm sections. Haematoxylin and eosin or AZAN-Mallory staining was performed on serial sections[5,23]. Myocyte cross-sectional area was measured by tracing the outline of 100–200 myocytes in each section[5,23]. For immunohistochemical analysis, frozen heart sections (5 μm) were fixed in buffered 4% paraformaldehyde. The antibodies used were anti-mouse CD45 (ANASPEC), CD68 (Serotec), Ly6G/6C (BD Pharmingen), CD3 (Abcam), LAMP2a (Zymed), LC3 (ref. 25) and TLR9 (Santa-Cruz). For *in situ* hybridization analysis, the mouse IL-6 (1-636) and IL-1β (1-810) RNA probes were labelled using a DIG RNA Labelling Kit and detected using a DIG Nucleic Acid Detection Kit (Roche Diagnostics). For immunoelectron microscopy, frozen heart tissue was embedded in LR White resin and the deposited DNA was detected using anti-DNA antibody (Abcam) and immunogold conjugated anti-mouse IgG (British Biocell International)[26]. For DNA detection, heart sections were incubated in PicoGreen (Molecular Probes) for 1 h. We used EdU to detect mitochondrial DNA in the heart section. Twenty-four hours before TAC, mice were injected intraperitoneally with 250 μg of EdU every 2 h five times, and EdU was detected using a Click-iT EdU Alexa Fluor 488 Imaging Kit (Invitrogen).

***In vitro and in vivo* rescue experiments with the TLR9 inhibitor.** Adult mouse cardiomyocytes were isolated from 12- to 14-week-old male mouse hearts as we previously described[5]. Cardiomyocytes were pre-treated with 1 μg ml^{-1} inhibitory CpG oligodeoxynucleotides (ODN2088) (Operon) (5′-TCCTGGCGGGGAAGT-3′) or control oligodeoxynucleotides (ODN2088 control) (5′-TCCTGAGCTTGAAGT-3′) for 5 h and incubated with 20 nM CCCP or 50 μM isoproterenol for 24 h (ref. 20). Cell death was estimated by Trypan blue staining[5]. To monitor mitochondrial membrane potential ($\Delta\psi$), the cells were loaded with tetramethylrhodamine ethyl ester (Molecular Probes) at 10 nM for 30 min before observation. In *in vivo* study, the mice were injected intravenously with 500 μg of the oligodeoxynucleotides 2 h before and 2 days after TAC, and they were analysed 4 days after TAC. To estimate survival, the mice received additional administration of the oligodeoxynucleotides 4 days after TAC and every 3 days thereafter.

Statistical analysis. Results are shown as the mean ± s.e.m. Paired data were evaluated using a Student's *t*-test. A one-way analysis of variance with the Bonferroni post hoc test was used for multiple comparisons. The Kaplan–Meier method with a log-rank test was used for survival analysis.

CORRIGENDUM

doi:10.1038/nature11515

Corrigendum: Mitochondrial DNA that escapes from autophagy causes inflammation and heart failure

Takafumi Oka, Shungo Hikoso, Osamu Yamaguchi, Manabu Taneike, Toshihiro Takeda, Takahito Tamai, Jota Oyabu, Tomokazu Murakawa, Hiroyuki Nakayama, Kazuhiko Nishida, Shizuo Akira, Akitsugu Yamamoto, Issei Komuro & Kinya Otsu

Nature **485,** 251–255 (2012); doi:10.1038/nature10992

In this Letter, several images were mistakenly switched or duplicated during preparation of the artwork. In Figs 1f and 2a, the sham-operated *Dnase2a*$^{-/-}$ and TAC-operated *Dnase2a*$^{+/+}$ mice panels were switched. In Fig. 4d, the panel showing CD3 staining for ODN2088 control-treated TAC-operated *Dnase2a*$^{+/+}$ mice (now shown correctly as black-bordered panel in Fig. 1 below) is a duplicate of that showing Ly6G staining for ODN2088-treated TAC-operated *Dnase2a*$^{-/-}$ mice. The panel showing CD45 staining for ODN2088-treated TAC-operated *Dnase2a*$^{+/+}$ (now shown correctly as blue-bordered panel in Fig. 1 below) was prepared from the original picture of ODN2088 control-treated TAC-operated *Dnase2a*$^{+/+}$. In Supplementary Fig. 4c, sham-operated *Dnase2a*$^{-/-}$ and TAC-operated *Dnase2a*$^{+/+}$ mice panels were switched. Finally, in Supplementary Fig. 10d, the panels showing CD3 and Ly6G staining for sham-operated *Tlr9*$^{+/+}$ mice were switched. These corrections do not alter any of the conclusions of this Letter, and the authors apologize for any confusion these errors may have caused.

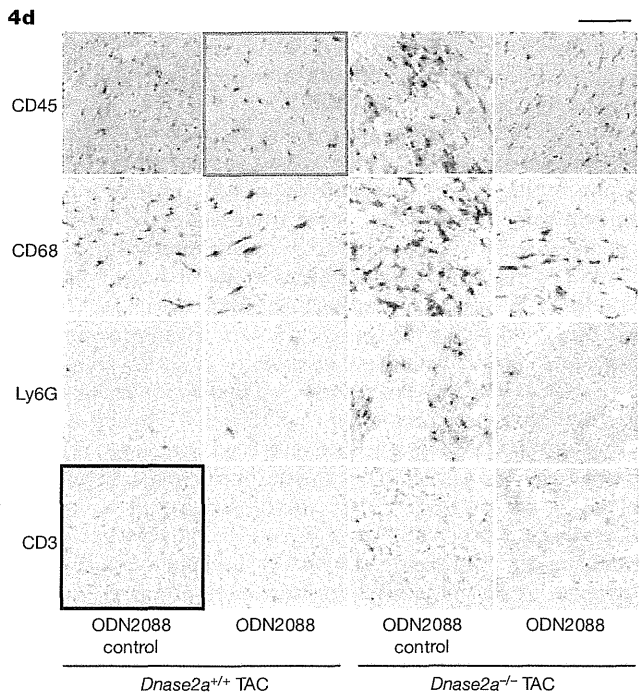

Figure 1 | This is the corrected Fig. 4d of the original Letter.

Renal collecting duct epithelial cells regulate inflammation in tubulointerstitial damage in mice

Katsuhito Fujiu,[1,2] Ichiro Manabe,[1,3] and Ryozo Nagai[1,2,3,4]

[1]Department of Cardiovascular Medicine, [2]Translational Systems Biology and Medicine Initiative, [3]Global COE, and [4]Translational Research Center, the University of Tokyo Graduate School of Medicine, Tokyo, Japan.

Renal tubulointerstitial damage is the final common pathway leading from chronic kidney disease to end-stage renal disease. Inflammation is clearly involved in tubulointerstitial injury, but it remains unclear how the inflammatory processes are initiated and regulated. Here, we have shown that in the mouse kidney, the transcription factor Krüppel-like factor–5 (KLF5) is mainly expressed in collecting duct epithelial cells and that *Klf5* haploinsufficient mice (*Klf5*$^{+/-}$ mice) exhibit ameliorated renal injury in the unilateral ureteral obstruction (UUO) model of tubulointerstitial disease. Additionally, *Klf5* haploinsufficiency reduced accumulation of CD11b^{+}F4/80^{lo} cells, which expressed proinflammatory cytokines and induced apoptosis among renal epithelial cells, phenotypes indicative of M1-type macrophages. By contrast, it increased accumulation of CD11b^{+}F4/80^{hi} macrophages, which expressed CD206 and CD301 and contributed to fibrosis, in part via TGF-β production — phenotypes indicative of M2-type macrophages. Interestingly, KLF5, in concert with C/EBPα, was found to induce expression of the chemotactic proteins S100A8 and S100A9, which recruited inflammatory monocytes to the kidneys and promoted their activation into M1-type macrophages. Finally, assessing the effects of bone marrow–specific *Klf5* haploinsufficiency or collecting duct– or myeloid cell–specific *Klf5* deletion confirmed that collecting duct expression of *Klf5* is essential for inflammatory responses to UUO. Taken together, our results demonstrate that the renal collecting duct plays a pivotal role in the initiation and progression of tubulointerstitial inflammation.

Introduction

The incidence of end-stage renal disease is increasing worldwide and represents a growing clinical and economic burden. Regardless of whether renal injury begins in the glomeruli or within the tubulointerstitium, tubulointerstitial damage is a common feature of all chronic progressive renal diseases and is considered to be the final common pathway leading from chronic kidney disease to end-stage renal disease (1–3). In cases of chronic kidney disease, inflammation is a critical mechanism that promotes closely interlinked fibrosis and cellular injury within the tubulointerstitium (4), and macrophages are the predominant infiltrating immune cells mediating that inflammatory process (3). Earlier studies have suggested that proteinuria, renal hypoxia, and/or glomerulus-derived cytokines may induce macrophage recruitment to the kidneys. However, it remains unclear which cell types responds to pathological stimuli and activate inflammatory processes in the kidney, though proximal tubular epithelial cells have been shown to produce the chemokine MCP-1 (3).

Macrophages infiltrating the kidneys produce various proinflammatory cytokines, including TNF-α and IL-1β, as well as metalloproteinases (3). Moreover, the finding that blockade of TNF-α and IL-1β suppresses glomerular inflammation and ameliorates renal damage suggests the infiltrating macrophages contribute in some way to the renal injury (5). Macrophage infiltration also often correlates with the degree of renal fibrosis, and depletion of macrophages reduces fibrosis in several disease models, suggesting that macrophages also contribute to fibrosis (6). On the other hand, macrophages that take up apoptotic cells exhibit antiinflammatory properties and may contribute to resolution of inflammation (7). Indeed, hepatic macrophages were shown to be important for resolution of inflammatory scarring (8). Thus, macrophages likely play multiple, and often opposing, roles in kidney disease and repair (6).

Recent studies demonstrating the diversity of macrophage phenotypes and functionality suggest that the activation state of macrophages may determine their pathogenic or reparative roles in kidney disease (9). In vitro studies have shown that Th1 cytokines, alone or in concert with microbial products, elicit classical M1 activation of macrophages, while Th2 cytokines (IL-4 and IL-13) elicit an alternative form of activation designated M2 (9, 10). M2 macrophages are thought to suppress immune responses and promote tissue remodeling (6, 9, 10), though M2 activation is a rather generic term used to describe various forms of macrophage activation other than classic M1. In addition, the diversity of macrophage activation has been established primarily based on in vitro findings (10), and the phenotypes and functions of M2-type macrophages in vivo are still poorly understood. Very recently it was shown that some, but not all, kidney macrophages exhibit surface expression of Ly-6C (11), which means the macrophage population involved in the renal response to injury is a heterogeneous one. However, the specific functions of the different macrophage subsets are not yet clear.

The renal collecting ducts contribute to the control of water and electrolyte balance. Collecting duct epithelial cells express the water channel aquaporin-2 (AQP2) in their apical plasma membrane and AQP3 and AQP4 in their basolateral membrane (12). Water is transported across the collecting duct epithelium

Conflict of interest: The authors have declared that no conflict of interest exists.
Citation for this article: *J Clin Invest.* 2011;121(9):3425–3441. doi:10.1172/JCI57582.

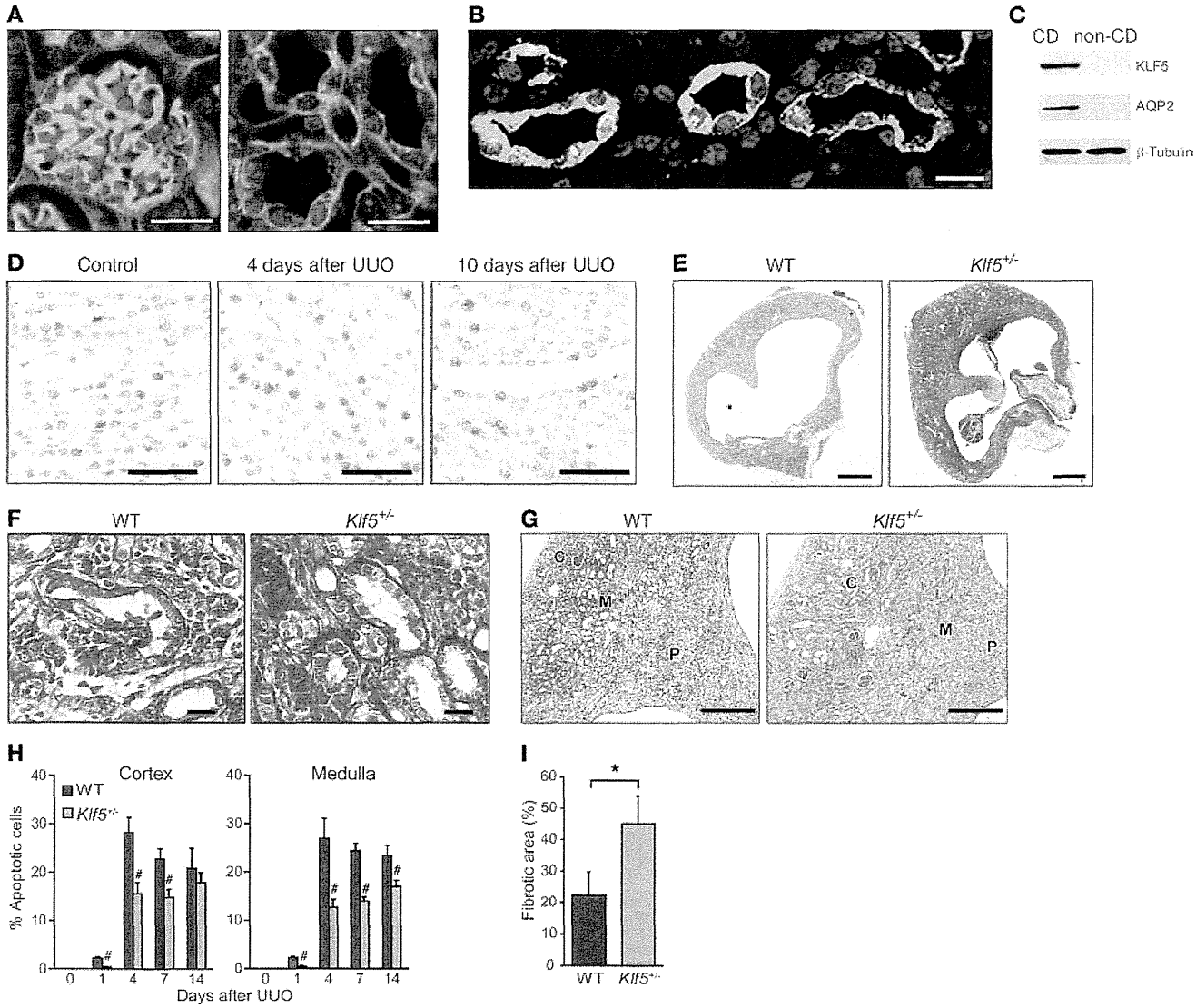

Figure 1

KLF5 is involved in UUO-induced renal injury. (**A**) Immunohistochemical staining of KLF5 (red) in mouse kidneys. Left and right panels show portions of the cortex and medulla, respectively. Nuclei and cell membranes were stained using DAPI (blue) and wheat germ agglutinin (green), respectively. Scale bars: 20 μm. (**B**) KLF5 expression was confined to AQP2-expressing collecting duct cells in papilla. KLF5 (red), AQP2 (green), and nuclei (blue) are shown. Scale bar: 20 μm. (**C**) Expression of KLF5 protein in the collecting duct. Collecting duct (CD) cells were isolated from kidneys by centrifugal separation. The remaining renal cells were non-CD cells. β-Tubulin served as a loading control. (**D**) UUO-induced upregulation of KLF5 in the collecting duct. KLF5 (brown) was detected by immunostaining of sections of medulla under basal conditions (control) and at the indicated times after UUO. Scale bars: 50 μm. (**E–G**) Masson's trichrome (**E** and **F**) and H&E (**G**) staining of wild-type and *Klf5*$^{+/-}$ kidneys 14 days after UUO. C, cortex; M, medulla; P, papilla. Scale bars: 1 mm (**E**), 20 μm (**F**), 500 μm (**G**). (**H**) Apoptotic cell fractions in kidneys from wild-type and *Klf5*$^{+/-}$ mice at the indicated days after UUO. Apoptotic cells were analyzed by TUNEL staining, as shown in Supplemental Figure 3A. $^{\#}P < 0.05$ versus wild-type at the same time point. $n = 6$. (**I**) Fibrotic area stained with picrosirius red 14 days after UUO. $^{*}P < 0.05$. $n = 6$. Representative sections are shown in Supplemental Figure 3C.

through those AQPs. AQP2 is abundantly expressed in the connecting tubule (connecting tubule cells), in the cortical and outer medullary collecting ducts (principal cells), and in the inner medullary collecting duct (IMCD cells) and plays an essential role in urinary concentration. Recent studies have shown that collecting duct cells in culture (13, 14) and in the fetal urinary tract obstruction model (15) exhibit a loss in epithelial phenotypes and a concomitant gain in mesenchymal phenotypes through a process often termed "epithelial-mesenchymal transition." This suggests that collecting duct cells are in some way involved in interstitial fibrosis. However, it remains largely unknown whether or how collecting duct cells contribute to tubulointerstitial inflammation.

Members of the Krüppel-like factor (KLF) family of transcription factors are important regulators of development, cellular differentiation, and growth, as well as the pathogenesis of various diseases, including cancer and cardiovascular disease (16). We previously

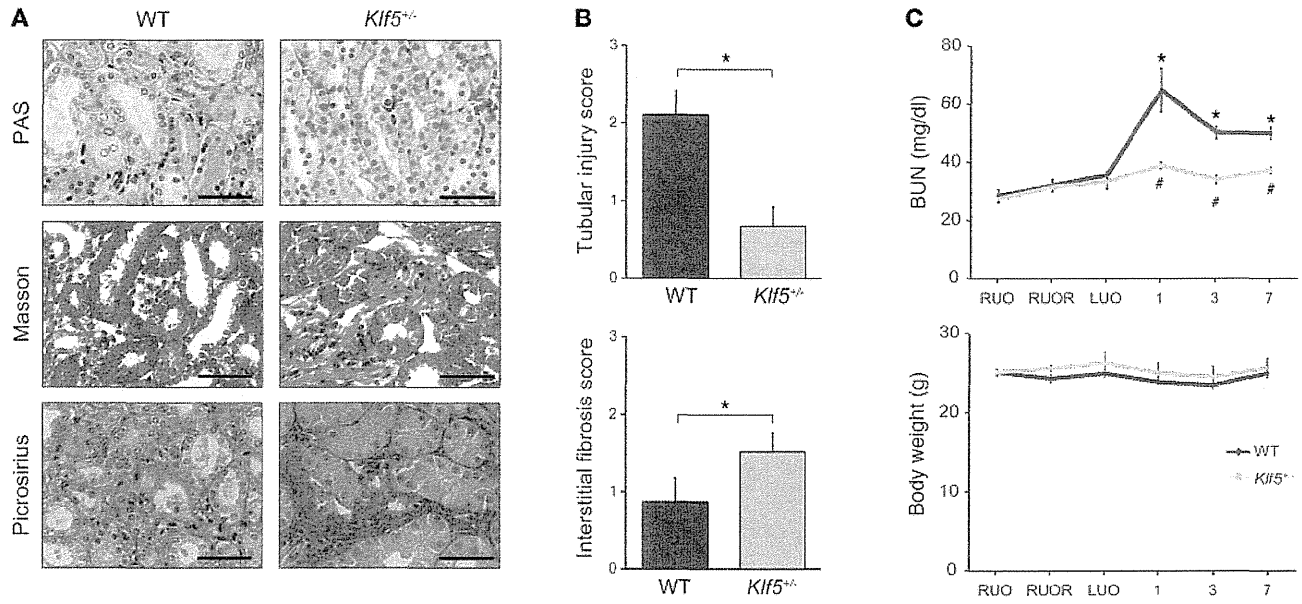

Figure 2

Klf5 haploinsufficiency ameliorated renal dysfunction induced by the reversible UUO. The right ureters of *Klf5*$^{+/-}$ and wild-type mice were transiently obstructed for 3 days; then 7 days after relief of the obstruction, the left ureters were obstructed. (**A**) Representative PAS, Masson's trichrome, and picrosirius red staining of wild-type and *Klf5*$^{+/-}$ right kidneys 7 days after left ureter obstruction. Scale bars: 50 μm. (**B**) Tubular injury and interstitial fibrosis scores are shown. $^{*}P < 0.05$. (**C**) BUN and body weight were measured prior to right ureteral obstruction (RUO), prior to release of the obstruction (RUOR), prior to left ureteral obstruction (LUO), and on indicated days after LUO. $n = 7$ for each group. $^{*}P < 0.05$ versus the baseline of the same genotype. $^{\#}P < 0.05$ versus wild-type at the same time point.

showed that KLF5 expressed in cardiac fibroblasts is required for the cardiac hypertrophy and fibrosis that develop in response to continuous infusion of angiotensin II and pressure overload (17, 18). KLF5 also plays a central role in arterial wall remodeling (17, 19). With these results as background, we were interested in whether KLF5 plays a role in renal tubulointerstitial inflammation and fibrosis. We found that *Klf5*$^{+/-}$ mice were protected from renal injury induced by unilateral ureteral obstruction (UUO), but showed enhanced fibrosis. Through a combination of in vitro and in vivo analyses, we further show that collecting duct epithelial cells respond to UUO and initiate the accumulation of M1-type macrophages at least in part through KLF5-dependent production of the secretory proteins S100A8 and S100A9. Our findings demonstrate a previously unappreciated function of collecting duct epithelial cells as central regulators of tubulointerstitial inflammatory processes.

Results

Klf5 is expressed in collecting duct epithelial cells. We first analyzed the distribution of *Klf5* expression in the kidney. Immunohistochemical staining showed that, in normal kidneys, KLF5 is expressed in the nuclei of collecting duct epithelial cells, but not in glomeruli or other tubules (Figure 1A). Consistent with this finding, expression of KLF5 was restricted to cells also expressing AQP2, which is known to be specifically expressed in collecting duct epithelial cells (ref. 20, Figure 1B, and Supplemental Figure 1A; supplemental material available online with this article; doi:10.1172/JCI57582DS1). The collecting duct epithelial cell-specific expression of KLF5 was still further confirmed by its presence in collecting duct cells isolated from kidneys and its absence in non-collecting duct cells (Figure 1C and Supplemental Figure 1B).

Klf5 haploinsufficiency ameliorates renal injury and dysfunction induced by UUO. We next employed the UUO model of tubulointerstitial damage to analyze the role of KLF5 in renal injury (21). We found that UUO increased KLF5 expression in renal collecting duct cells (Figure 1D and Supplemental Figure 1C). Expression of *Klf5* mRNA was readily detected in collecting duct cells, but was barely detectable in CD11b^{+}F4/80^{+} (monocytes/macrophages), CD31^{+} (endothelial cells), or α-SMA^{+} (myofibroblasts, mesangial cells, and smooth muscle cells) cells sorted from kidneys (Supplemental Figure 1C). Upon immunohistochemical staining, KLF5 was detected only in collecting duct cells in sections of normal and day 4 UUO kidneys; a few interstitial cells also stained positive for KLF5 in sections of day 10 UUO kidneys (Figure 1D). These results indicate that high-level *Klf5* expression is largely limited to collecting duct cells.

Under physiological conditions, *Klf5*$^{+/-}$ mice did not exhibit renal dysfunction or pathological changes (Supplemental Figure 2A and Supplemental Table 1). However, when *Klf5*$^{+/-}$ mice were subjected to UUO, they exhibited less renal structural destruction than wild-type mice, as indicated by amelioration of tubular dilation and atrophy, tubular epithelial cell sloughing, and tubular basement membrane thickening (Figure 1, E–G, and Supplemental Figure 2B). Consequently, kidney weight loss and tubular injury score were significantly lower in *Klf5*$^{+/-}$ than wild-type mice (Supplemental Figure 2C). Moreover, significantly fewer apoptotic cells were observed in both the cortex and medulla of kidneys from *Klf5*$^{+/-}$ compared with wild-type mice (Figure 1H and Supplemental Figure 3, A and B). In sharp contrast, interstitial fibrosis was significantly exacerbated in *Klf5*$^{+/-}$ mice, as compared with wild-type mice (Figure

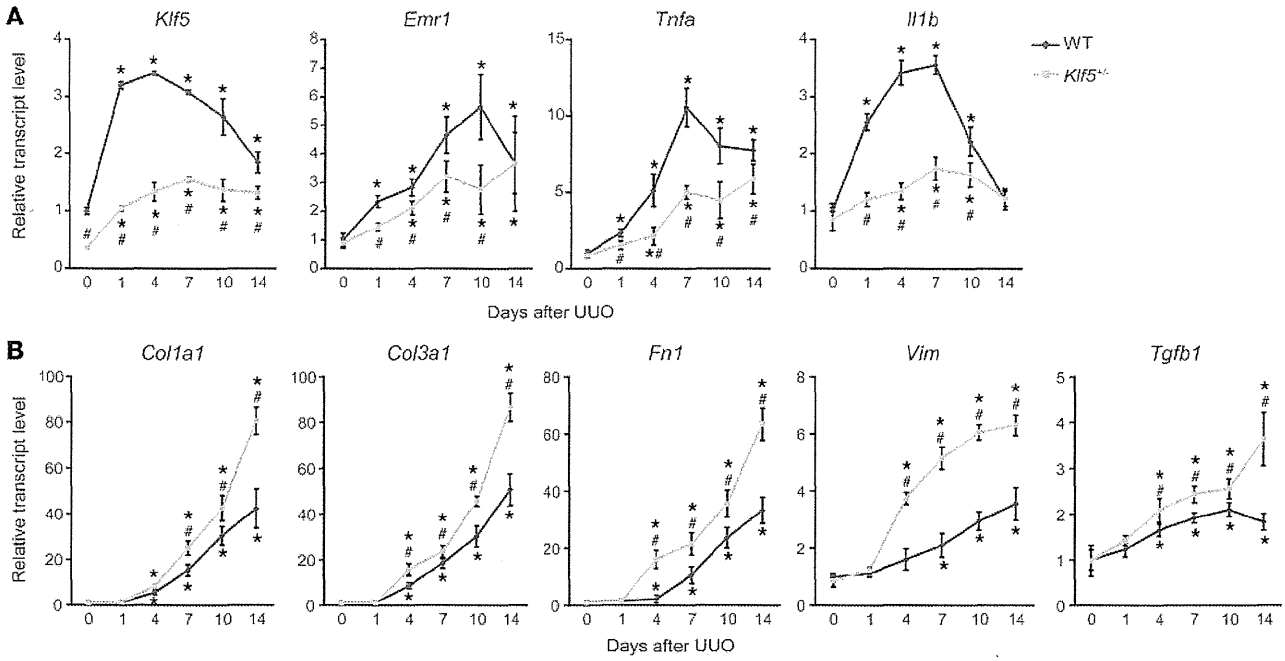

Figure 3

Effects of *Klf5* haploinsufficiency on renal gene expression. Wild-type and *Klf5*$^{+/-}$ mice were subjected to UUO, after which relative transcript levels of genes involved in renal inflammation (**A**) and fibrosis (**B**) were measured at the indicated times using real-time PCR. Data labeled day 0 show gene expression in kidneys under basal conditions. Expression levels were normalized first to those of 18s rRNA and then further normalized to the levels in the kidneys from control wild-type mice. *$P < 0.05$ versus the control (day 0) for the same genotype; #$P < 0.05$ versus wild-type at the same time point. $n = 5$ for each point.

1, E, F, and I, Supplemental Figure 2C, and Supplemental Figure 3, C and D). It thus appears that the *Klf5* haploinsufficiency protected kidneys from the structural destruction induced by UUO, but it promoted fibrosis. Because the contralateral kidneys were uninjured, neither wild-type nor *Klf5*$^{+/-}$ mice showed abnormal blood chemistry, and no mice died within 3 months after UUO (Supplemental Table 2).

To analyze the effects of *Klf5* haploinsufficiency on renal dysfunction, we employed a reversible UUO procedure (22). Initially, the right ureter was obstructed for 3 days, and then the obstruction was released. After mice were allowed to recover for 7 days, the left ureter was ligated to disable contralateral kidney function. After an additional 7 days, the right kidneys of *Klf5*$^{+/-}$ mice exhibited less renal injury than those of wild-type mice (Figure 2, A and B), though fibrosis was more pronounced in the *Klf5*$^{+/-}$ kidney. Blood urea nitrogen (BUN) levels were significantly lower in *Klf5*$^{+/-}$ than wild-type mice, while body weights were not different (Figure 2C). These results demonstrate that *Klf5* haploinsufficiency protected kidneys from dysfunction induced by the transient UUO, despite the apparent augmentation in fibrosis.

Klf5 haploinsufficiency modulates renal inflammation and fibrosis induced by UUO. Recent studies suggest that inflammation is crucially involved in renal cellular injury and fibrosis (23). This prompted us to assess the involvement of KLF5 in inflammatory processes in the kidney. We found that, in wild-type mice, UUO increased renal expression of *Tnfa* and *Il1b*, which encode the proinflammatory cytokines TNF-α and IL-1β, respectively (Figure 3A); that the expression levels were highest 7 days after UUO; and that the levels of these proinflammatory cytokines were significantly reduced in *Klf5*$^{+/-}$ kidneys following UUO. In wild-type kidneys, UUO also increased expression of *Emr1*, which encodes the macrophage marker F4/80, and that effect was significantly reduced in *Klf5*$^{+/-}$ kidneys, suggesting that UUO-induced renal infiltration by macrophages and their inflammatory activation are diminished in *Klf5*$^{+/-}$ kidneys. As expected from the enhanced fibrosis, expression levels of *Col1a1* and *Col3a1*, encoding collagen type I and III, respectively; *Fn1*, encoding fibronectin; *Vim*, encoding vimentin; and *Acta2*, encoding α-SMA, were all significantly increased in *Klf5*$^{+/-}$ kidneys, and their expression was highest 14 days after UUO (Figure 3B). In addition, expression of *Tgfb1*, which encodes the profibrotic cytokine TGF-β1, was also significantly increased in *Klf5*$^{+/-}$ kidneys. As a result, the interstitial area in *Klf5*$^{+/-}$ kidneys was reduced after UUO due to a reduction in the number of apoptotic cells, whereas the fibrotic area and the fibrotic/interstitial area ratio were increased in *Klf5*$^{+/-}$ kidneys (Supplemental Figure 3D). Collectively, these results suggest that *Klf5* haploinsufficiency suppresses early inflammatory processes following UUO, while augmenting fibrotic processes at later times.

Differential recruitment of macrophage subtypes to kidneys after UUO. The reduction in F4/80 expression observed in *Klf5*$^{+/-}$ kidneys suggests that macrophage accumulation was suppressed there. We tested that idea using flow cytometry to assess renal macrophages (Supplemental Figure 4A). In wild-type mice, UUO induced accumulation of CD11b^{+}F4/80^{+} cells (Figure 4A), and we noted two major subpopulations: CD11b^{+}F4/80^{lo} (R1) and CD11b^{+}F4/80^{hi} (R2). Under basal conditions the CD11b^{+}F4/80^{hi} fraction was significantly larger than the CD11b^{+}F4/80^{lo} fraction (Figure 4B), but the latter was increased from day 1 after UUO, while the former

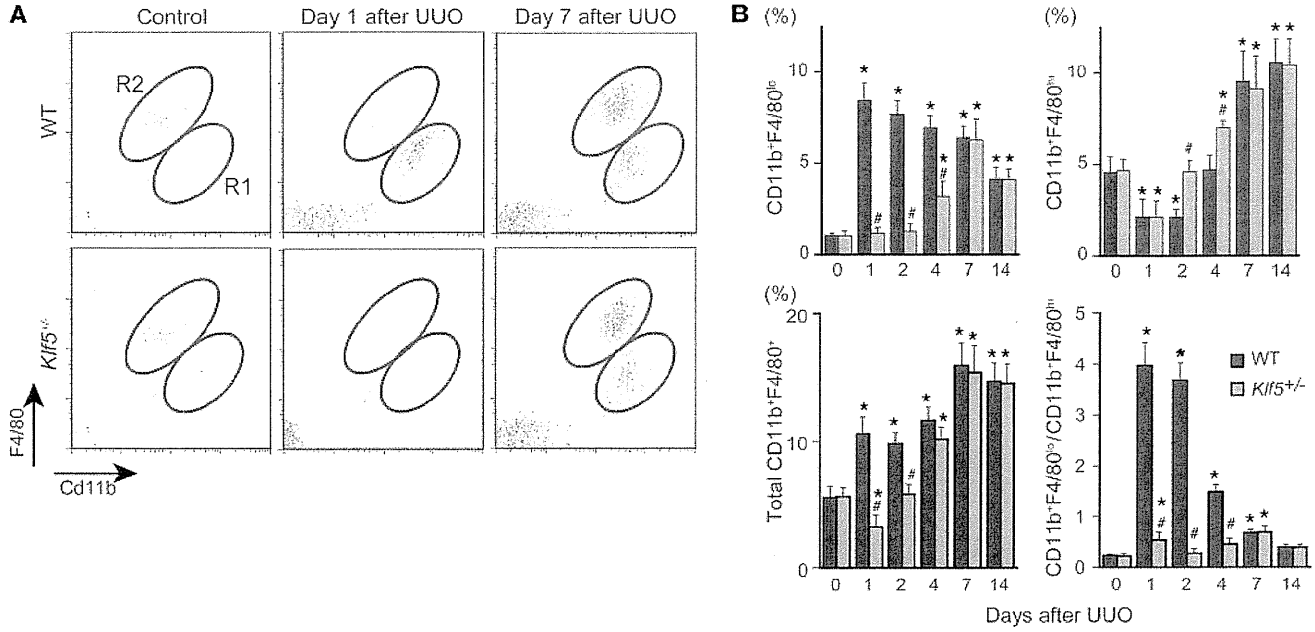

Figure 4

KLF5 controls the recruitment and accumulation of CD11b$^+$F4/80$^+$ cells in response to UUO. (**A**) Representative flow cytometry plots of macrophages in whole kidneys from wild-type and *Klf5*$^{+/-}$ mice subjected to either UUO or sham operation. R1 and R2 indicate CD11b$^+$F4/80^{lo} and CD11b$^+$F4/80^{hi} cells, respectively. (**B**) Fractions of CD11b$^+$F4/80^{lo} (region R1 in **A**), CD11b$^+$F4/80^{hi} (R2), and total CD11b$^+$F4/80$^+$ cells among total live cells and the ratios of CD11b$^+$F4/80^{lo} to CD11b$^+$F4/80^{hi} cells isolated from the kidneys of wild-type and *Klf5*$^{+/-}$ mice subjected to UUO. $^*P < 0.05$ versus day 0 of the same genotype; $^\#P < 0.05$ versus wild-type at the same time point. $n = 6$ for each group. The cell populations expressed as fractions of total macrophages and numbers of cells per kidney are shown in Supplemental Figure 5, A and B.

was reduced on days 1 and 2. As a result, the ratio of CD11b$^+$F4/80^{lo} to CD11b$^+$F4/80^{hi} cells was significantly increased from day 1 to day 7. The cell ratio then declined to the basal level within 14 days after UUO.

We next characterized the surface phenotypes of CD11b$^+$F4/80$^+$ cells and found that while CD11b$^+$F4/80^{lo} cells were Ly-6C$^+$, CD11b$^+$F4/80^{hi} cells were Ly-6C$^{-/lo}$, and majorities of both cell populations were negative for the granulocyte marker Ly-6G (Supplemental Figure 4B). They were also negative for the myeloid-derived suppressor cell marker CD93 (24). In addition, while both CD11b$^+$F4/80^{lo} and CD11b$^+$F4/80^{hi} cells showed greater forward scatter (FSC) on day 7 than day 1 after UUO, CD11b$^+$F4/80^{hi} cells showed much greater FSC than CD11b$^+$F4/80^{hi} cells on day 7 (Supplemental Figure 4C). In Cytospin preparations, CD11b$^+$F4/80^{lo} cells exhibited a small, monocytoid morphology on day 1 but also included larger cells by day 7 (Supplemental Figure 4D). In contrast, CD11b$^+$F4/80^{hi} cells were larger than CD11b$^+$F4/80^{lo} cells and had a fried egg–like morphology. Despite their monocytoid morphology, day-1 CD11b$^+$F4/80^{lo} cells showed higher surface F4/80 and CD11b levels than circulating CD11b$^+$Ly-6C$^+$ inflammatory monocytes, which have been shown to be recruited to kidneys after UUO (11). This suggests CD11b$^+$F4/80^{lo} cells include macrophages as well as monocytes that had been recruited to the kidneys, where they are undergoing differentiation into macrophages (11, 25), while CD11b$^+$F4/80^{hi} cells are more mature macrophages. Moreover, CD11b$^+$F4/80^{hi} cells but not CD11b$^+$F4/80^{lo} cells were positive for CD206 and CD301, markers of M2-type activation. Collectively then, the two populations of CD11b$^+$F4/80$^+$ cells in UUO kidneys exhibited a CD11b$^+$F4/80^{lo}Ly-6C$^+$CD206$^-$ CD301$^-$ phenotype, which is indicative of M1-type activation, and a CD11b$^+$F4/80^{hi}Ly-6C$^{-/lo}$Ly-6G$^-$CD206$^+$CD301$^+$ phenotype, which is indicative of M2-type activation (11, 26).

Under basal conditions there were no significant differences in the CD11b$^+$F4/80^{lo} and CD11b$^+$F4/80^{hi} fractions between wild-type and *Klf5*$^{+/-}$ kidneys (Figure 4B and Supplemental Figure 5, A and B). However, *Klf5*$^{+/-}$ kidneys contained significantly fewer CD11b$^+$F4/80^{lo} cells from day 1 to day 4 after UUO. By contrast, *Klf5*$^{+/-}$ kidneys contained more CD11b$^+$F4/80^{hi} cells on days 2 and 4 than wild-type kidneys (Figure 4B and Supplemental Figure 5, A and B). As a result, the CD11b$^+$F4/80^{lo} to CD11b$^+$F4/80^{hi} ratio was significantly higher than baseline only on days 1 and 7 in *Klf5*$^{+/-}$ kidneys. Reduced inflammatory monocyte/macrophage infiltration into *Klf5*$^{+/-}$ kidneys 1 day after UUO was further confirmed by immunohistochemical staining for F4/80 and Ly-6C (Supplemental Figure 5, C and D). Taken together, these findings suggest that CD11b$^+$F4/80^{lo} and CD111b$^+$F4/80^{hi} cells differentially accumulate in the kidney during the course of the response to UUO. At early times, when apoptosis and tissue destruction are occurring, primarily CD11b$^+$F4/80^{lo} monocytes/macrophages accumulate in kidneys. Later, when tissue remodeling and fibrosis dominate, the numbers of CD11b$^+$F4/80^{hi} macrophages are increased. *Klf5* haploinsufficiency reduces accumulation of CD11b$^+$F4/80^{lo} cells and increases CD11b$^+$F4/80^{hi} cells at earlier time points, thereby altering the balance of macrophage polarity during the response to UUO.

Renal CD11b$^+$F4/80$^+$ cells are phenotypically different from splenic classical DCs. DCs have been identified in kidneys (27–29). Although CD11c has been used to distinguish renal DCs from macrophages (30), the marker is widely expressed and is induc-

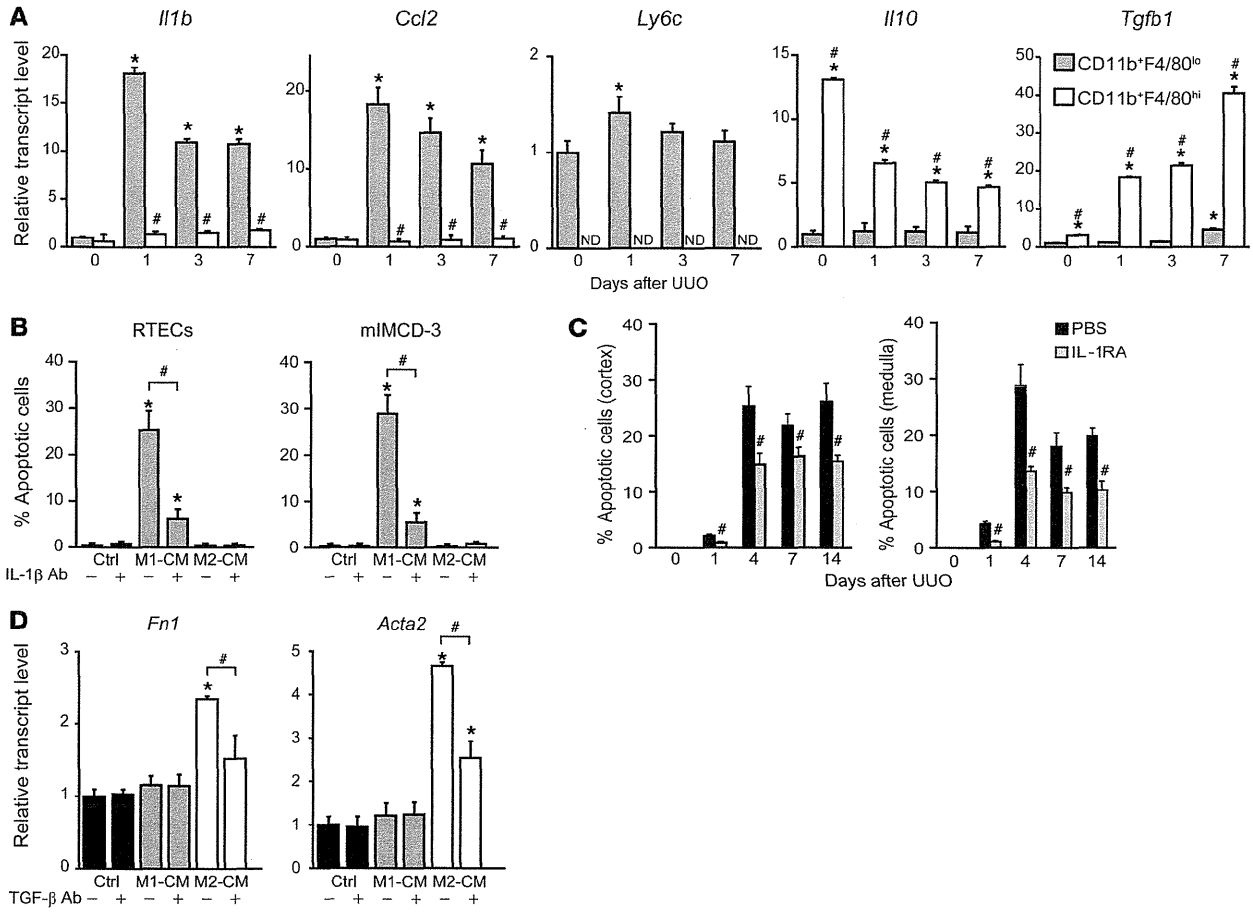

Figure 5

Differential involvement of CD11b$^+$F4/80^{lo} and CD11b$^+$F4/80^{hi} cells in renal responses to UUO. (**A**) mRNA expression in CD11b$^+$F4/80^{lo} and CD11b$^+$F4/80^{hi} cells isolated from kidneys under basal conditions (day 0) or after UUO. Expression levels were normalized to those of 18s rRNA and then further normalized to the levels in the resident CD11b$^+$F4/80^{lo} cells isolated from normal kidneys of wild-type mice. $n = 3$. $^{\#}P < 0.05$ versus CD11b$^+$F4/80^{lo} cells from wild-type mice at the same time point. $^*P < 0.05$ versus day 0 of the same population. ND, nondetectable. (**B**) Effects of conditioned medium (CM) prepared by incubating CD11b$^+$F4/80^{lo} or CD11b$^+$F4/80^{hi} cells isolated from kidneys 1 (CD11b$^+$F4/80^{lo}) or 7 (CD11b$^+$F4/80^{hi}) days after UUO in serum-free RPMI medium for 24 hours. Serum-free RPMI containing 0.3% BSA was used as a control medium (Ctrl). Fractions of TUNEL$^+$ apoptotic primary mouse RTECs and mIMCD-3 cells after culture in the CM with either control IgG or IL-1β neutralizing antibody for 24 hours. $n = 6$. Expression levels were normalized to those of 18s rRNA and then further normalized to the levels in cells treated with the control medium. $^*P < 0.05$. versus cells in control medium with control IgG; $^{\#}P < 0.05$. (**C**) Effects of IL-1RA administration on UUO responses. Renal phenotypes of wild-type mice intraperitoneally administered either PBS (vehicle) or IL-1RA (200 μg daily). $^{\#}P < 0.05$ versus the PBS group at the same time point. $n = 6$. (**D**) Levels of *Fn1* and *Acta2* transcription in 10T1/2 embryo fibroblasts cultured for 24 hours in CM as in **B** with either control IgG or TGF-β neutralizing antibody. $^*P < 0.05$ versus cells in control medium with control IgG; $^{\#}P < 0.05$. $n = 3$.

ible in macrophages and other immune cells during inflammation (31). To better characterize renal CD11b$^+$ cells in comparison with bona fide DCs, we assessed the expression of multiple DC markers in renal CD11b$^+$ cells and splenic classical DCs (Supplemental Figure 6). We found that CD11b$^+$F4/80^{lo} cells were CD11c^{lo}MHCII$^{-/+}$CD86$^-$CD83$^-$, which supports the notion that they are monocytes/macrophages. CD11b$^+$F4/80^{hi} cells were CD11c^{int}MHCII$^+$CD86$^+$CD83$^-$. As compared with splenic classical DCs, CD11c levels were lower in renal CD11b$^+$F4/80^{hi} cells, and CD83, a marker for mature DCs (32, 33), was not expressed. In Cytospin preparations, CD11b$^+$F4/80^{hi} cells contained vacuolar cytoplasm and lacked cytoplasmic extensions, which are macrophage-like characteristics and different from those of splenic DCs (Supplemental Figure 4D and Supplemental Figure 7A). These results indicate that renal CD11b$^+$F4/80^{hi} cells express several DC markers, but their phenotypes differ from those of splenic classical DCs.

Because we were not able to identify a cell population that resembled splenic DCs among the CD11b$^+$ cells, we tested whether cells expressing high levels of CD11c might be present among the renal leukocytes (CD45$^+$ cells). We found that CD11c^{hi} cells were present and were CD11c^{hi}MHCII$^+$CD86$^+$CD83$^+$CD11b$^-$F4/80^{lo}, which is a phenotype that closely resembles that of splenic DCs (Supplemental Figure 6D). In Cytospin preparations, moreover, renal CD11c^{hi} cells had pleomorphic nuclei and cytoplasmic extensions, and were morphologically similar to splenic DCs (Supplemental Figure 7B). The renal CD11c^{hi}MHCII$^+$CD83$^+$ cells were widely distributed on FSC/side scatter (SSC) plots, and the majority was found

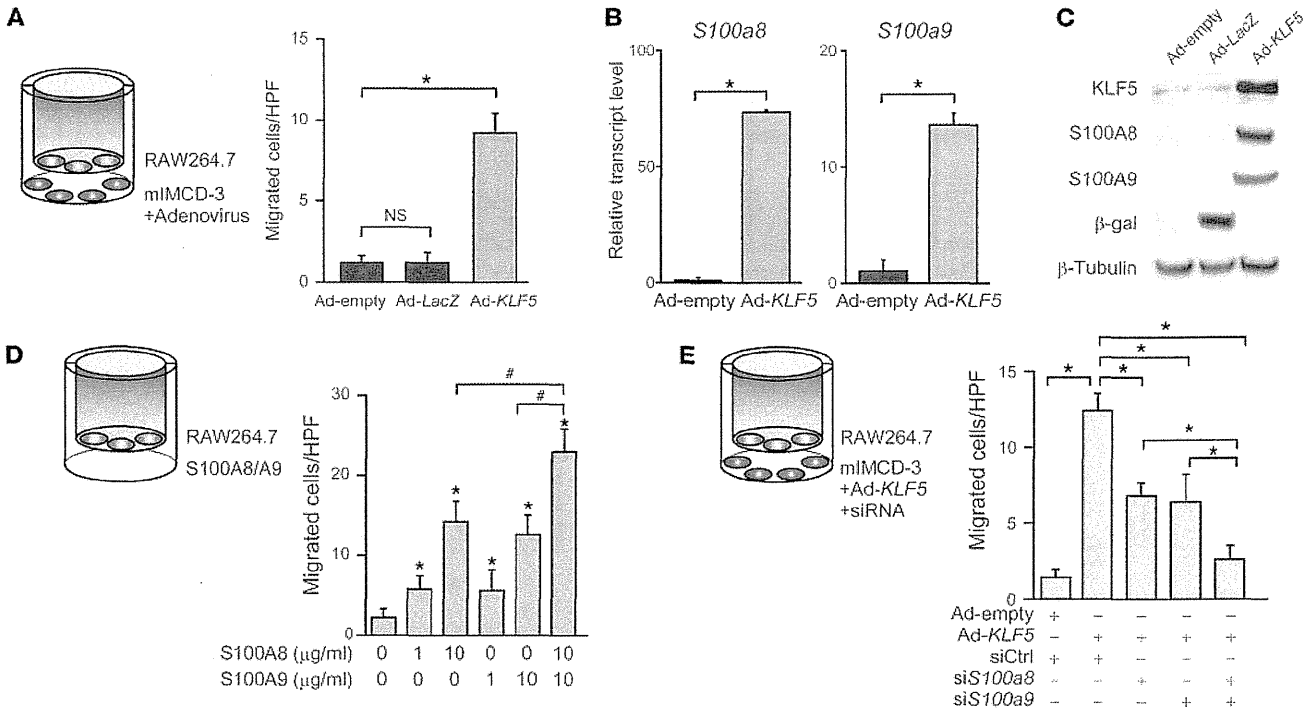

Figure 6

KLF5 induces accumulation of M1 macrophages via S100A8 and S100A9. (**A**) Activation of RAW264.7 macrophage migration by mIMCD-3 cells overexpressing KLF5. As shown schematically, mIMCD-3 and RAW264.7 cells were plated in the bottom wells and inserts, respectively. The mIMCD-3 cells were infected with empty adenovirus (Ad-empty), adenovirus expressing β-galactosidase (Ad-*LacZ*), or adenovirus expressing KLF5 (Ad-*KLF5*), as indicated. The numbers of cells that migrated through the porous membranes per high-power field (HPF) during the 8-hour incubation are shown. $n = 12$. $^*P < 0.05$. (**B** and **C**) Levels of *S100a8* and *S100a9* transcription in mIMCD-3 cells overexpressing KLF5. Relative levels of *S100a8* and *S100a9* transcripts were determined by real-time PCR (**B**). $n = 6$. $^*P < 0.05$. In **C**, expression of KLF5, S100A8, S100A9 protein and β-galactosidase were assessed by Western blotting. β-Tubulin was used as a loading control. (**D**) Effects of recombinant S100A8 and S100A9 on RAW264.7 cell migration. Recombinant S100A8 and/or S100A9 were added to the medium in the lower wells, as shown. $n = 6$. $^*P < 0.05$ versus migrated cells without S100 proteins; $^\#P < 0.05$. (**E**) Effects of *S100a8* and/or *S100a9* knockdown in mIMCD-3 cells overexpressing KLF5 on RAW264.7 migration. mIMCD-3 cells overexpressing KLF5 were transfected with siRNAs against *S100a8* and *S100a9* or control siRNA (siCtrl), as indicated, after which they were plated in the bottom wells, as shown. The numbers of RAW264.7 cells that migrated during the 8-hour incubation are shown. $n = 6$. $^*P < 0.05$.

outside of the R3 gate that was used to characterize CD11b$^+$ cells (Supplemental Figures 4A and 7C), indicating that these cells were not included in our CD11b$^+$F4/80^{hi} and CD11b$^+$F4/80^{lo} cell populations. In addition, the renal CD11c^{hi}MHCII$^+$CD83$^+$ cell fractions were not affected by UUO or *Klf5* haploinsufficiency, making it unlikely that these cells contribute to the renal phenotypes observed in *Klf5*$^{+/-}$ mice (Supplemental Figure 7D). Collectively then, it appears that kidneys contain a CD11c^{hi}MHCII$^+$CD83$^+$ cell population that closely resembles classical DCs. By contrast, the surface marker profile and cellular morphology of CD11b$^+$F4/80^{hi} cells are different from those of classical DCs. Because they differ from both splenic classical DCs and renal classical DC-like cells, and more resemble tissue macrophages in other tissues (34), we will refer to CD11b$^+$F4/80^{hi} cells as macrophages hereafter.

CD11b$^+$F4/80^{lo} and CD11b$^+$F4/80^{hi} cells differentially affect epithelial and mesenchymal cells. To analyze the functions of renal CD11b$^+$F4/80$^+$ cells in more detail, we isolated them from kidneys at various times after UUO (Supplemental Figure 8A). Analysis of mRNA expression in CD11b$^+$F4/80^{lo} and CD11b$^+$F4/80^{hi} cells isolated 0, 1, 3, and 7 days after UUO showed that levels of *Il1b* and *Ccl2* transcripts, encoding the proinflammatory cytokines IL-1β and MCP-1, respectively, were much higher in CD11b$^+$F4/80^{lo} than CD11b$^+$F4/80^{hi} cells (Figure 5A), suggesting that CD11b$^+$F4/80^{lo} cells promote inflammation. *Ly6c* was expressed in CD11b$^+$F4/80^{lo} cells, but was undetectable in CD11b$^+$F4/80^{hi} cells. By contrast, CD11b$^+$F4/80^{hi} cells showed higher levels of *Il10* and *Tgfb1* transcripts, encoding the antiinflammatory cytokines IL-10 and TGF-β1, respectively, which suggests the CD11b$^+$F4/80^{hi} M2-type macrophages are involved in fibrosis and resolution of inflammation. However, CD11b$^+$F4/80^{hi} cells did not express two other M2 markers, *Ym1* and *Fizz1* (data not shown), indicating that the characteristics of CD11b$^+$F4/80^{hi} cells do not perfectly match those of the M2 macrophages previously studied in vitro (9).

To further investigate the functional differences between CD11b$^+$F4/80^{lo} and CD11b$^+$F4/80^{hi} cells, we incubated cultured primary mouse renal tubular epithelial cells (RTECs) and mIMCD-3 mouse collecting duct epithelial cells in medium conditioned by either CD11b$^+$F4/80^{lo} or CD11b$^+$F4/80^{hi} cells isolated from kidneys subjected to UUO. The surface phenotypes and cytokine gene expression profiles of CD11b$^+$F4/80^{lo} and CD11b$^+$F4/80^{hi} cells cultured for 24 hours were similar to those of the cells just after

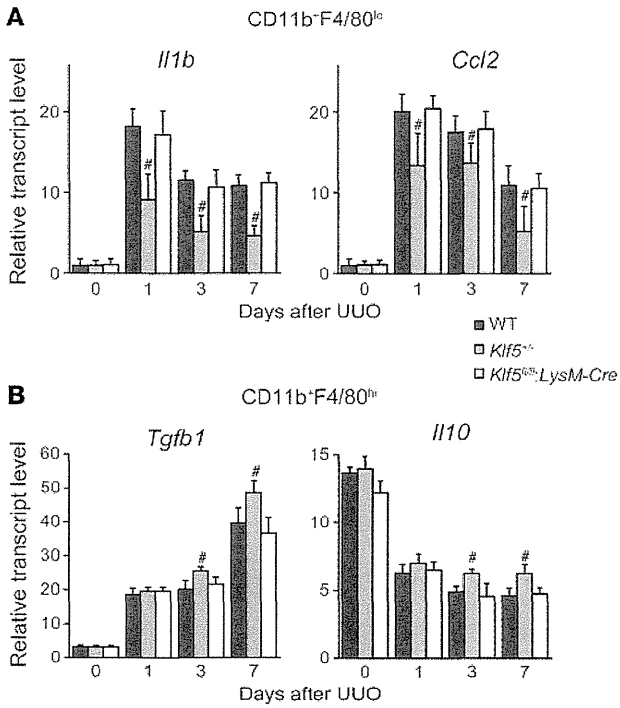

Figure 7

Effects of global and macrophage-specific *Klf5* deletion on macrophage cytokine gene expression. Expression of cytokine genes in CD11b$^+$F4/80^{lo} (**A**) and CD11b$^+$F4/80^{hi} (**B**) cells isolated from kidneys of wild-type, *Klf5*$^{+/-}$, and *Klf5*$^{fl/fl}$;*LysM-Cre* mice at indicated days after UUO. Expression levels were normalized to those of 18s rRNA and then further normalized to the levels in cells in wild-type kidney under basal conditions. $n = 3$. $^{\#}P < 0.05$ versus cells of wild-type mice at the same time point.

isolation (Supplemental Figure 8, B and C). We observed much higher frequencies of apoptosis among RTECs and mIMCD-3 cells in medium conditioned by CD11b$^+$F4/80^{lo} cells than among those in medium conditioned by CD11b$^+$F4/80^{hi} macrophages (Figure 5B). In fact, the CD11b$^+$F4/80^{hi}-conditioned medium induced apoptosis in very few cells. Moreover, the proapoptotic effect of CD11b$^+$F4/80^{lo}-conditioned medium was significantly suppressed by an anti–IL-1β neutralizing antibody. In line with these in vitro observations, inhibition of IL-1 receptor signaling by IL-1 receptor antagonist (IL-1RA) suppressed renal injury and renal cell apoptosis in UUO (Figure 5C and Supplemental Figure 9). The CD11b$^+$F4/80^{hi}-conditioned medium induced expression of *Fn1* and *Acta2*, encoding fibronectin 1 and α-SMA, in C3H10T1/2 mouse embryonic fibroblasts, which is indicative of the cells' activation into myofibroblasts, and this myofibroblastic differentiation was significantly suppressed by an anti–TGF-β neutralizing antibody (Figure 5D). These results demonstrate that CD11b$^+$F4/80^{lo} monocytes/macrophages induce renal epithelial cell injury via inflammatory cytokines, including IL-1β, whereas CD11b$^+$F4/80^{hi} M2-type macrophages appear to promote fibrosis by inducing myofibroblastic differentiation, at least in part, via TGF-β.

KLF5 controls expression of S100A8 and S100A9, which induce migration and M1 activation in macrophages. The results summarized so far suggest that renal KLF5 is involved in the accumulation of CD11b$^+$F4/80^{lo} monocytes/macrophages in the kidney. To test this possibility directly, we cultured mIMCD-3 cells infected with KLF5-expressing (Ad-*KLF5*), β-galactosidase–expressing (Ad-*LacZ*), or empty (Ad-empty) adenoviral vector in the bottom wells of Boyden chambers, and cultured RAW264.7 macrophages in the upper inserts (Figure 6A). The mIMCD-3 cells overexpressing KLF5 induced migration of significantly larger numbers of RAW264.7 cells than the cells infected with Ad-*LacZ* or empty adenovirus. This suggests that KLF5 controls production of chemoattractants. Similarly, overexpression of KLF5 in mIMCD-3 cells promoted migration of BM-derived macrophages (BMDMs) (Supplemental Figure 10A). The BMDMs had been treated with either IFN-γ/LPS or IL-4 to induce M1 or M2 activation, respectively (35), and KLF5 overexpression in mIMCD-3 cells induced migration of more M1-activated BMDMs than M2-activated BMDMs.

We then sought the downstream KLF5 effector molecules mediating the observed macrophage migration. We identified potential KLF5 target genes by combining microarray analysis with ChIP followed by high-speed sequencing (ChIP-seq) of KLF5 binding sites. We first identified genes whose expression was upregulated by Ad-*KLF5* in mIMCD-3 cells (Supplemental Table 3) and then narrowed the range of candidate genes on the basis of whether the ChIP-seq reads were in the proximity of each gene locus. Two of the candidate KLF5 target genes were *S100a8* and *S100a9*. These genes encode the secretory proteins S100A8 and S100A9, which have been shown to induce leukocyte migration (36, 37). Quantitative real-time PCR and Western blot analyses confirmed upregulation of *S100a8* and *S100a9* expression in mIMCD-3 cells infected with Ad-*KLF5* (Figure 6, B and C).

When we then tested whether S100A8 or S100A9 was capable of recruiting macrophages to kidneys, we found that recombinant S100A8 or S100A9 increased migration of RAW264.7 cells and BMDMs in Boyden chambers (Figure 6D and Supplemental Figure 10B) and that knocking down *S100a8* and/or *S100a9* significantly reduced RAW264.7 and BMDM migration induced by overexpression of KLF5 in mIMCD-3 cells (Figure 6E and Supplemental Figure 10, C and D). Both S100A8 and S100A9 more efficiently induced migration of M1-activated BMDMs than M2-activated BMDMs (Supplemental Figure 10B). Thus, S100A8 and S100A9 appear to be important chemoattractants controlled by KLF5.

In addition to the suppressed accumulation of CD11b$^+$F4/80^{lo} cells in *Klf5*$^{+/-}$ kidneys after UUO (Figure 4B), the CD11b$^+$F4/80^{lo} cells present expressed lower levels of *Il1b* and *Ccl2* than wild-type cells (Figure 7A). By contrast, expression of *Il10* and *Tgfb1* in CD11b$^+$F4/80^{hi} M2-type macrophages was increased in *Klf5*$^{+/-}$ kidneys (Figure 7B). Lin et al. recently demonstrated that circulating CD11b$^+$Ly-6C$^+$ monocytes differentiate into both M1- and M2-type macrophages in UUO kidneys (11), suggesting that the renal microenvironment plays an important role in the differential activation of macrophages. Taking this in consideration, our results suggest that *Klf5* haploinsufficiency may render the renal microenvironment relatively suppressive for M1-type activation but more permissive for M2-type activation. We therefore hypothesized that S100A8 and S100A9 might also mediate M1-type activation in UUO kidneys. To test this idea, we treated BMDMs with S100A8 and S100A9 (Figure 8A). We found they induced expression of the M1 markers *Il1b* and *Tnfa*, while the M2 markers *Arg1* and *Mrc1* (CD206) were unaffected, indicating that S100A8/A9 can induce M1-type activation of BMDMs.

S100A8 and S100A9 mediate accumulation and activation of macrophages in kidneys in vivo. To determine whether S100A8 and S100A9 also induce macrophage accumulation in kidneys in vivo, we directly injected recombinant S100A8 and S100A9 into the kidneys of mice, where they clearly induced accumulation of CD11b$^+$F4/80^{lo}